

An Accurate 10 m Annual Crop Map Product of Maize and Soybean Across the United States

Haijun Li¹, Xiao-Peng Song^{1, *}, Bernard Adusei¹, Jeffrey Pickering¹, Andre Lima¹, Andrew Poulson¹, Antoine Baggett¹, Peter Potapov^{1,2}, Ahmad Khan¹, Viviana Zalles^{1,2}, Andres Hernandez-Serna¹, Samuel M. Jantz^{1,3}, Amy H. Pickens¹, Carolina Ortiz-Dominguez¹, Xinyuan Li¹, Theodore Kerr¹, Zhen Song¹, Svetlana Turbanova¹, Eddy Bongwele¹, Heritier Koy Kondjo¹, Anna Komarova¹, Stephen V. Stehman⁴, Matthew C. Hansen¹

¹Department of Geographical Sciences, University of Maryland, College Park, MD 20742, United States

²World Resources Institute, Washington, DC, 20002, United States

³National Institute for Modeling Biological Systems, University of Tennessee, Knoxville, TN 37996, United States

⁴Department of Sustainable Resources Management, SUNY College of Environmental Science and Forestry, Syracuse, NY 13210, United States

Correspondence to: Xiao-Peng Song (xpsong@umd.edu)

Abstract High-resolution crop maps over large spatial extents are fundamental to many agricultural applications; however, generating high-quality crop maps consistently across space and time remains a challenge. In this study, we improved a workflow for crop mapping and developed [the first](#) openly available, annual, 10-m spatial resolution maize and soybean map [products](#) over the Contiguous United States (CONUS) from 2019 to 2022 ([available at the website of the Global Land Analysis and Discovery \(GLAD\) team at the University of Maryland \(https://glad.umd.edu/dataset/mapping-crops-10-m-resolution-united-stateshttps://glad.umd.edu/projects/mapping_crops_10_m_resolution_united_states\)](#)). We obtained all available Sentinel-2 surface reflectance data between May and October for every year, applied quality assurance, corrected the bidirectional reflectance distribution function (BRDF) effects, and generated 10-day analysis ready data (ARD) composites. We then derived multi-temporal metrics from the 10-day ARD as training features for the national-scale wall-to-wall mapping. We implemented a stratified, two-stage cluster sampling, and then conducted annual field surveys and collected ground data. Utilizing the training data with Sentinel-2 multi-temporal metrics and topographic factors, we trained random forest models generalized for annual maize and soybean classification separately. Validated using field data from the two-stage cluster sample, our annual maps achieved consistent overall accuracies (OA) greater than 95% with standard errors of less than 1%. User's accuracies (UAs) and producer's accuracies (PAs) for maize were higher than 91% and 84% across the years, and UAs and PAs for soybean were greater than 88% and 82%, respectively. To illustrate the substantial improvement of the 10-m map over existing datasets, e.g., the 30-m Cropland Data Layer (CDL), we aggregated the 10-m maps to 30-m spatial resolution and quantified the [amount](#) of [30-m](#) mixed pixels that can be reduced [by improving the mapping from 30 m to 10 m at field, regional, and national levels](#). The counties with the most maize and soybean production in Iowa, Illinois and Nebraska had the lowest reduction in mixed pixels, ranging from 1% to [74%](#), whereas southern counties had a higher reduction in mixed pixels. Overall, the median percentages of mixed maize and soybean pixels reduction across all counties were [84%](#)

34 and 9+6%, respectively. With more Sentinel-2-like data available from continuous observations and incoming satellite
35 missions, we anticipate that 10-m crop maps will greatly benefit long-term monitoring for agricultural practices from the field
36 to global scales. The dataset is also available at
37 <https://doi.org/10.6084/m9.figshare.28934993.v2><https://doi.org/10.6084/m9.figshare.28934993.v1> (Li et al., 2025)

38 1 Introduction

39 Satellite-derived crop maps are essential to many agricultural applications, such as crop yield prediction (Bolton and Friedl,
40 2013; Song et al., 2022; Wang et al., 2024), food market forecasting (Tanaka et al., 2023), crop area estimation (Khan et al.,
41 2016), conservation policy design (Song et al., 2021b; Zalles et al., 2021), smallholder livelihood evaluation (Lambert et al.,
42 2018), warfare impacts on food security (Li et al., 2022; Lin et al., 2023), and greenhouse gas emissions in agriculture (Escobar
43 et al., 2020; Ouyang et al., 2023). However, along with these benefits are the outstanding challenges to generating high-quality
44 crop maps, including developing consistent ready-to-use satellite datasets, collecting representative field data, and building
45 classification algorithms robust to phenological variations.

46 Dense time series of satellite observations with complete spatial coverage is essential to mapping crops at broad scales. With
47 global coverage and daily revisit frequency, the Moderate Resolution Imaging Spectroradiometer (MODIS) data are often used
48 for crop mapping in early studies (Wardlow et al., 2007; Wardlow and Egbert, 2008). However, spatial details within individual
49 small fields can rarely be depicted at 250-m resolution (Fritz et al., 2015), especially for more than 475 million smallholder
50 and family farms accounting for 12% of the world's agricultural land (Lowder et al., 2016). Since the opening of the Landsat
51 archive in 2008 (Woodcock et al., 2008), Landsat data have been extensively used to generate 30-m crop maps in many parts
52 of the world, such as in North America (Boryan et al., 2011; Fisetete et al., 2013; Johnson and Mueller, 2021; Song et al., 2017;
53 Wang et al., 2020), Europe (Foerster et al., 2012), South America (Song et al., 2021b), and Asia (Dong et al., 2016; Khan et
54 al., 2021; Remelgado et al., 2020). However, Landsat-based crop mapping is hampered by the relatively sparse 16-day temporal
55 frequency (8 days with two satellites), especially when cloudy weather persists. Compared to Landsat, Sentinel-2A and -2B
56 together have a revisit frequency of 5 days and provide 10-m, 20-m and 60-m spectral bands including red edge bands that are
57 particularly useful for crop identification (Immitzer et al., 2016; Song et al., 2021a). These advantages make Sentinel-2 data
58 one of the best publicly accessible data sources for crop mapping (Ghassemi et al., 2022; Han et al., 2021; Luo et al., 2022;
59 You et al., 2021).

60 Crop classification from satellite imagery is usually implemented by relating specific crop types to remotely sensed features,
61 using reference data and classification algorithms such as conventional machine learning or advanced deep learning (e.g.,
62 Alami Machichi et al., 2023; Joshi et al., 2023). Therefore, *in situ* data can serve as critical references to annotate satellite
63 imagery for supervised classifications, although field surveys over large areas require extensive time and labor resources.
64 Currently, the US Department of Agriculture (USDA) National Agricultural Statistics Service (NASS) collects periodic field

65 data across the US and produces the Cropland Data Layer (CDL) annually based on a large amount of ground data and
66 supervised algorithms (Boryan et al., 2011). When current-year labels are unavailable, some researchers have explored
67 transferring pre-trained models to target regions or years (Luo et al., 2022; Wang et al., 2019), or generating labels with
68 knowledge-guided approaches (Lin et al., 2022; You et al., 2023). However, these approaches are limited to experiments at
69 small spatial scales, such as the US Midwest and Northeast China, and thus the efficiency of national-scale crop classification
70 over large countries with more challenging environments remains to be explored. In cases where reference data are entirely
71 unavailable, unsupervised classifications are used first to cluster satellite-derived features and then assign crop labels to the
72 clusters to generate approximate crop maps (Konduri et al., 2020; Xiong et al., 2017). They, however, are vulnerable to outliers
73 and noisy features and require intensive visual inspections (Wang et al., 2019). In summary, collecting representative ground
74 data is a critical yet challenging component for large-area crop mapping.

75 Spatiotemporal consistency in crop classifications is necessary to make annual crop maps comparable and thus allow long-
76 term crop monitoring and change analysis. Yet this is undermined partly due to crop phenology variations across large extents,
77 depending on soil properties, planting dates, and weather conditions, among other factors (Deines et al., 2023; Yang et al.,
78 2017). On one hand, within a calendar year, crop progress is regionally different. To address this issue, some studies trained
79 regional models through agroecological zoning, which requires zone-specific training and validation (de Abelleira et al., 2020;
80 Wardlow and Egbert, 2008). On the other hand, yearly unaligned phenological profiles can jeopardize the classification
81 consistency across years, especially when extreme weather events occur (Manoochehr et al., 2021). Given these interannual
82 variations, classifiers that accurately identify crops in average normal growing seasons using single-date or time-series satellite
83 imagery may perform poorly for abnormal years. To this end, researchers proposed yearly specific classifications (Massey et
84 al., 2017; Som-ard et al., 2022). However, these annual models need fine-tuning based on reference data from each
85 corresponding year especially when encountering unseen growing trends, and thus cannot be generalized for long-term periods.

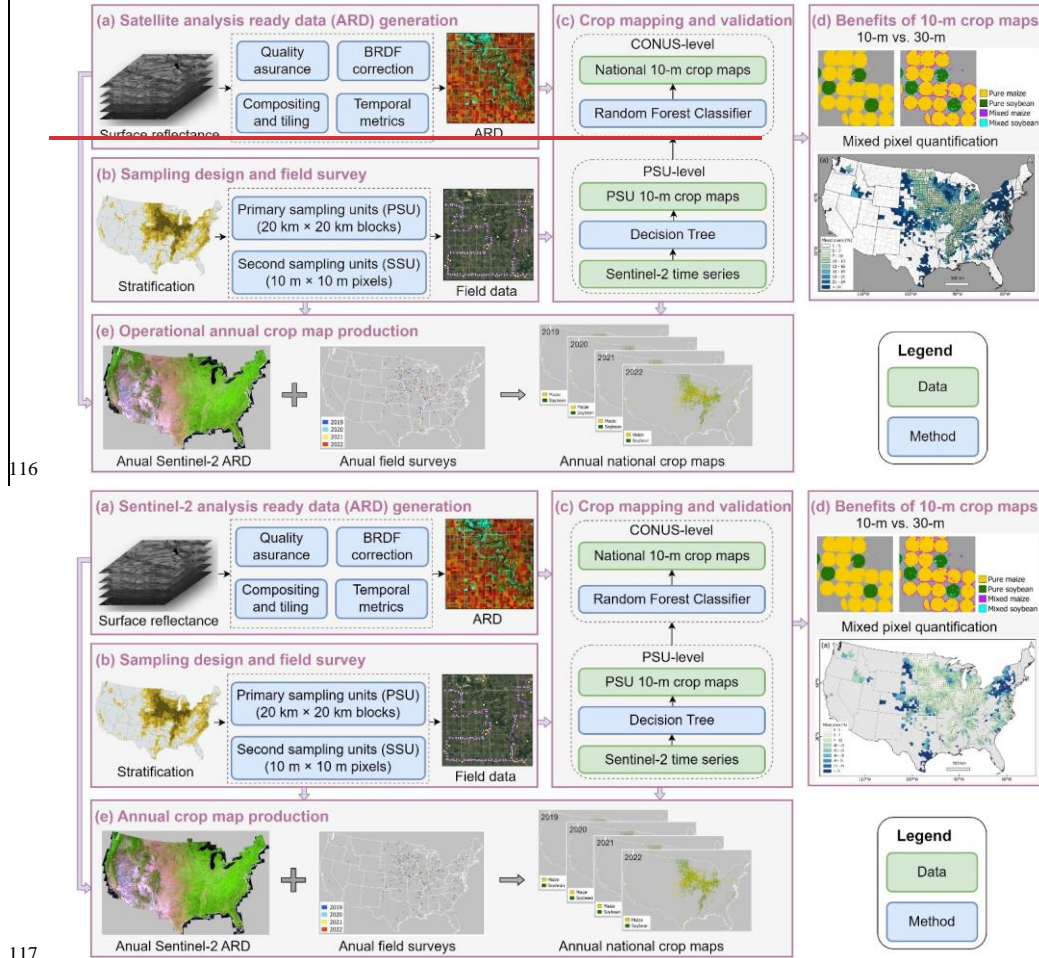
86 Multi-temporal metrics are statistical transformations of temporal profiles of satellite observations that can improve spatial
87 and temporal consistency and facilitate land cover mapping for large areas. In the mid-1980s, researchers derived phenological
88 features from pixel time series from the Advanced Very High Resolution Radiometer (AVHRR) for vegetation monitoring
89 (Malingreau, 1986) and from Landsat Multispectral Scanner (MSS) for crop classification (Badhwar, 1984). This metrics
90 method was then widely used for land cover mapping and change analysis from regional to global scales using AVHRR,
91 MODIS and Landsat data (DeFries et al., 1995; Hansen et al., 2013; Potapov et al., 2021b; Song et al., 2018). For crop mapping
92 over continental scales, the metrics method was used to generalize classification models robust to interannual phenological
93 variations (Song et al., 2021b). Many studies are adopting similar concepts for regional crop mapping (Kerner et al., 2022;
94 Konduri et al., 2020; Yang et al., 2023; Zhong et al., 2014).

95 In the US, the CDL has been used widely for many applications (Bolton and Friedl, 2013; Gao et al., 2017; Lobell et al., 2020;
96 Wright and Wimberly, 2013; Yan and Roy, 2016). Recently, the 2024 CDL has been successfully released with the spatial
97 resolution increased from 30 m to 10 m (https://www.nass.usda.gov/Research_and_Science/Cropland/SARS1a.php, accessed

98 [26 December 2025](#)). However, the [previous years of CDL are at 30-m resolution, and has have](#) inconsistent accuracies
99 depending on the location, and inaccurate classifications are observed in sparse or complex agricultural regions (Larsen et al.,
100 2015). The 30-m spatial resolution can lead to substantial mixed pixels, obscuring incremental or pixel-level changes,
101 particularly along field boundaries. In comparison, 10-m maps with a higher spatial resolution can improve the delineation of
102 precise field boundaries, reducing mixed pixels in individual fields, as well as lowering uncertainties of area estimation. [Global](#)
103 [10-m crop mapping efforts are rare, although the WorldCereal provides an example \(Van Tricht et al., 2023\)](#). In Europe, recent
104 10-m crop mapping efforts include the Crop Map of England (CROME) (CROME, 2024), the parcel-level crop maps in the
105 Netherlands (ESA, 2024), the crop maps produced by the Sentinel-2 for Agriculture (Sen2-Agri) (Defourny et al., 2019;
106 Inglada et al., 2015), [and the more recent High Resolution Layer Crop Types \(CTY\) \(EU, 2024⁴⁵\) and by WorldCereal \(Van](#)
107 [Fricht et al., 2023\)](#). In Asia, large-area crop-specific maps have been generated recently (Han et al., 2021; Li et al., 2023; Mei
108 et al., 2024). In the US, the potential of national-scale 10-m crop mapping has rarely been explored, although a recent
109 prototyping effort has been reported (Huang et al., 2024).

110 The objective of this study is to develop annual 10-m crop maps with Sentinel-2 time series. [We also and](#) quantify the benefits
111 of 10-m maps compared to [existing](#) 30-m products. In this study, we generated annual maize and soybean maps at 10-m spatial
112 resolution over the entire Contiguous US (CONUS), from 2019 to 2022. We also quantified the benefits of our 10-m crop
113 maps in mixed pixel reduction compared to 30-m maps, at field, regional and national scales. We improved a workflow

114 developed in previous studies (Li et al., 2023; Song et al., 2017) by combining satellite analysis ready data (ARD) generation,
 115 field survey design, and machine learning. An overview workflow for annual crop map production is presented in Figure 1.



117
 118 **Figure 1: Overview of the workflow for large-area annual crop map production.**

119 2 Materials and methods

120 2.1 Satellite analysis ready data (ARD) generation

121 Operational crop mapping over large areas relies on satellite data that are geometrically and radiometrically consistent with
122 quality assessment (e.g., Boryan et al., 2011; Fiset et al., 2013; Song et al., 2021b). Analysis ready data (ARD), defined by
123 the Committee on Earth Observation Satellites (CEOS), meet such criteria as “have been processed to a minimum set of
124 requirements and organized into a form that allows immediate analysis with a minimum of additional user effort and
125 interoperability both through time and with other datasets” (<https://ceos.org/ard/>, accessed 11 November 2024). To support
126 annual wall-to-wall crop mapping over the CONUS, we obtained all available Sentinel-2 data between May and October,
127 applied quality assurance, corrected the bidirectional reflectance distribution function (BRDF) effects, and generated 10-day
128 ARD composites.

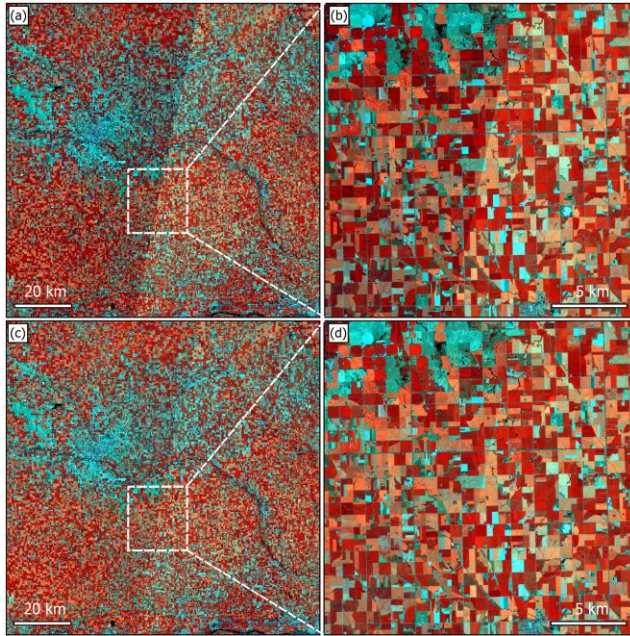
129 We downloaded Sentinel-2A and -2B Level-2A Bottom of the Atmosphere reflectance (S2 L2A) images from Google Cloud,
130 including the 10-m blue, green, red and near-infrared (NIR) bands, the 20-m red edge (RE1, RE2, RE3), narrow near-infrared
131 (NNIR) and shortwave infrared (SWIR1, SWIR2) bands. We selected images acquired between May 1 and October 31 after
132 filtering out images with > 80% cloud cover. We then processed all available Sentinel-2 data by utilizing the GLAD and
133 Zaratan high-performance computing clusters at the University of Maryland and generated Sentinel-2 ARD for the wall-to-
134 wall crop mapping. Details of the ARD generation are described in the following sections.

135 2.1.1 Quality assurance

136 Based on the S2 scene classification (SCL) layer, we generated the cloud mask by merging categories of cloud shadow, thin
137 cirrus, snow, cloud with low, medium and high probability into cloudy pixels. We also produced an additional cloud mask
138 layer derived from the Fmask algorithms (Zhu et al., 2015) and the Cloud Displacement Index (Frantz et al., 2018). We
139 combined the SCL-derived cloud mask with the additional cloud mask as the final quality assurance (QA) layer.

140 2.1.2 Bidirectional Reflectance Distribution Function (BRDF) correction

141 We corrected the BRDF effects using the c-factor method to derive nadir BRDF-adjusted reflectance (NBAR) (Roy et al.,
142 2017a, b). The S2 L2A product provides solar and view geometry metadata in 23×23 grids at 5-km spatial resolution. For
143 each multi-spectral instrument (MSI) detector in each spectral band, the solar zenith and azimuth angles remain consistent; the
144 view zenith and azimuth angles, however, vary from one detector to another, and from band to band. We calculated the mean
145 value of the view zenith and azimuth angle for each 5-km grid across all detectors and all spectral bands. Per-pixel solar and
146 view angles at 10-m resolution were derived by nearest neighbor interpolation of the 5-km grid values. As a result, the 10-m
147 angle layers were used to generate NBAR images using the global spectral BRDF model parameters (Roy et al., 2017a, b).
148 This process reduced the BRDF effects and improved the spatial coherence compared to the surface reflectance without BRDF
149 correction (Figure 2).



150
 151 **Figure 2:** Sentinel-2 false color composites (R: NIR, G: SWIR1, B: SWIR2) over a selected UTM tile 14TMP centered at (97.131°
 152 W, 41.942° N). (a-b) surface reflectance. (c-d) nadir BRDF-adjusted reflectance (NBAR). Two overlapping Sentinel-2B swaths
 153 acquired from orbit R112 on July 18, 2022 (backscattering direction) and orbit R012 on July 21, 2022 (forward scattering direction)
 154 were used. The orbit R112 data were overlaid on the orbit R012 data where they overlapped. All composites are displayed with the
 155 same stretch parameters.

156 2.1.3 Temporal composition and tiling

157 We resampled the 20-m bands to 10-m using the nearest neighbor method, applied the QA layer, and created 10-day median
 158 composites. For each NBAR band in a given 10-day interval, the median value of all clear-sky observations and the
 159 corresponding day of the year (DOY) were selected. We also implemented temporal linear interpolation on a per-pixel basis
 160 to fill the data gaps (Griffiths et al., 2019). For a missing value in a 10-day interval, the gap-filled value was calculated from
 161 the preceding and subsequent valid observations. A maximum of six 10-day intervals (i.e., 60 days or 2 months) was used to
 162 limit the period so that the interpolation was temporally relevant. For cases in which cloud-free observations are unavailable
 163 for two months, we did not conduct interpolation.

164 We divided the entire study area into $1^\circ \times 1^\circ$ non-overlapping tiles in geographic latitude/longitude projection with WGS84
 165 datum. Each tile was named by the latitude and longitude coordinates of the lower-left corner, with $0.0001^\circ \times 0.0001^\circ$ spatial

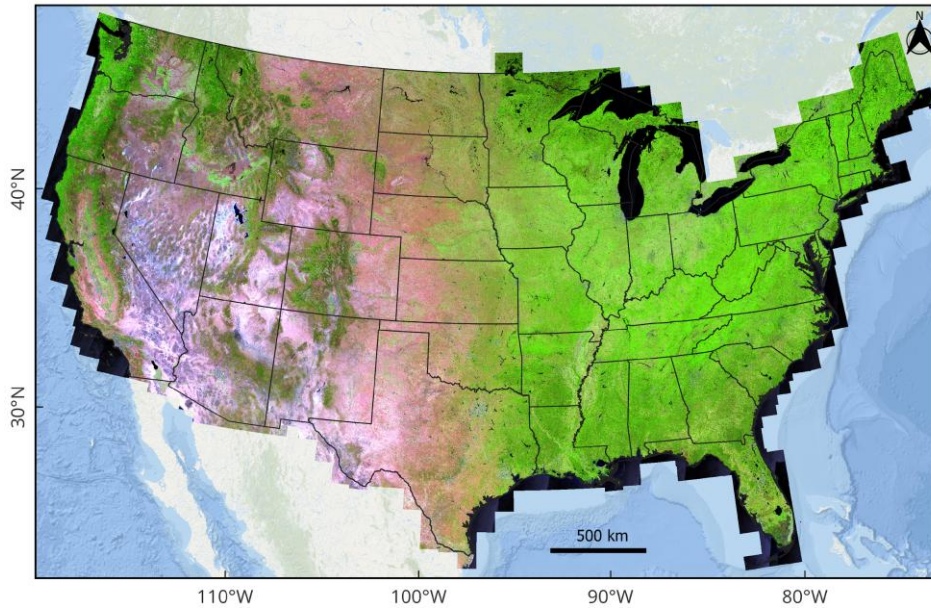
166 resolution to approximately match a 10-m pixel of Sentinel-2. We reprojected 1,028 Sentinel-2 Universal Transverse Mercator
167 (UTM) tiles into 939 $1^\circ \times 1^\circ$ tiles over the United States.

168 **2.1.4 Multi-temporal metrics**

169 The 10-day S2 ARD may have inconsistent observational frequencies across space and time depending on the geographical
170 location and cloud condition. Generating multi-temporal metrics from ARD can improve data consistency, and thus enable
171 large-area land cover mapping, which has been demonstrated in various applications at continental and global scales (Hansen
172 et al., 2013; Potapov et al., 2021; Song et al., 2021a).

173 Following the method in Potapov et al. (2020), we generated multi-temporal metrics from the 10-day S2 ARD (see Table S1).
174 First, we derived the Normalized Difference Vegetation Index (NDVI, $(\text{NIR} - \text{Red})/(\text{NIR} + \text{Red})$) (Tucker, 1979) and the
175 normalized ratio between shortwave infrared bands (SWSW, $(\text{SWIR1} - \text{SWIR2})/(\text{SWIR1} + \text{SWIR2})$) from corresponding
176 NBAR bands. Second, we ranked time-series observations by each NBAR band or index individually. We then selected the
177 second maximum, the second minimum, and median values per pixel, and calculated the 10th, 25th, 75th, and 90th percentiles.
178 We also calculated the average, standard deviation, and amplitude between these percentiles and the second maximum, the
179 second minimum values. Third, we ranked the observation day of year (DOYs) according to the time-series NDVI, and derived
180 values on the DOYs corresponding to the second maximum, the second minimum, and median, as well as the 10th, 25th, 75th,
181 and 90th percentiles of NDVI values. The average, standard deviation and amplitude were also calculated from these extracted
182 values.

183 In total, we calculated 621 metrics. The NBAR averages between the 25th and 75th percentiles from observations ranked by
184 individual bands are illustrated in Figure 3 and Figure 4a. The NBAR amplitudes reveal land surface phenology and thus
185 simplify visual interpretation of general land cover types such as cropland, open water, forest, and wetland (Figure 4b). When
186 the averages are calculated from observations with the highest NDVI values (between 90th percentile and the second maximum
187 NDVI value), the composite shows surface reflectance during the peak growing season, improving the identification of
188 multiple crop types (Figure 4c and Figure 4d).



189

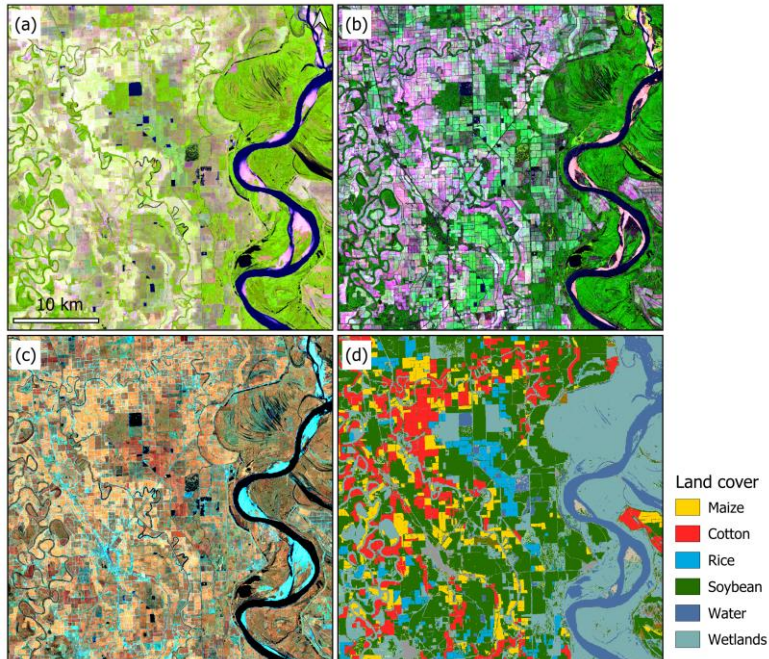
190

191

192

193

Figure 3: Sentinel-2 composites over the United States in 2022. The composites were created using the average value of nadir Bidirectional Reflectance Distribution Function (BRDF)-adjusted reflectance (NBAR) between the 25th and 75th percentiles from observations ranked by individual bands (R: SWIR1, G: NIR, B: Red). The original 10-m data are resampled to 250 m using the nearest neighbor for visualization purposes. The ESRI map is used as background.



194

195 **Figure 4: Composites of Sentinel-2 multi-temporal metrics in the Mississippi Valley.** (a) SWIR1-NIR-Red composite of NBAR
 196 average between the 25th and 75th percentiles from observations ranked by individual bands; (b) SWIR1-NIR-Red composite of
 197 NBAR amplitude between the second maximum and the second minimum values; (c) NIR-SWIR1-SWIR2 composites of average
 198 NBAR between the 90th percentile and the second maximum values from observations ranked by NDVI; (d) 2022 Cropland Data
 199 Layer. The coordinate of the center point is (91.312° W, 33.665° N). All panels are displayed in the same scale at 10-m resolution.

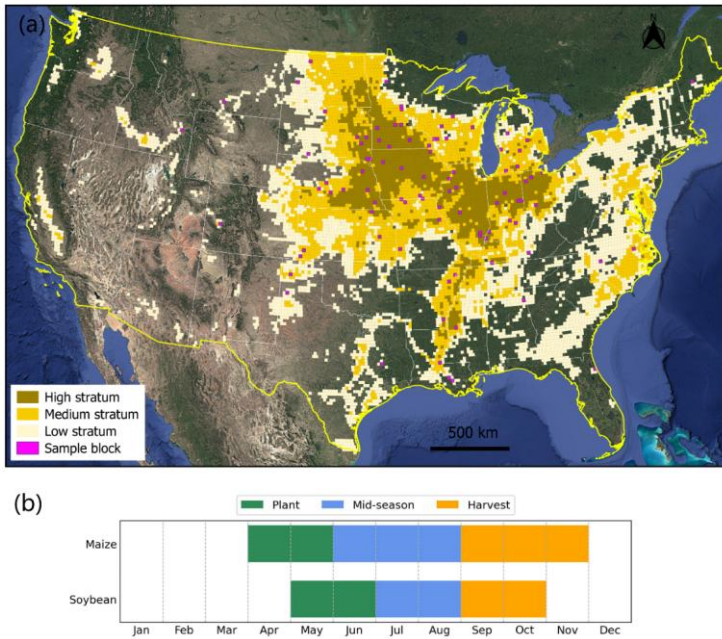
200 2.2 Sampling design and field survey

201 To support the 10-m crop mapping, we conducted extensive field surveys for *in situ* data collection, based on a two-stage
 202 cluster sampling design following Song et al. (2017). This approach has been demonstrated to be effective for agricultural
 203 applications in which ground reference data are collected at regional (Khan et al., 2018), national (King et al., 2017; Li et al.,
 204 2023), and continental (Song et al., 2021b) scales.

205 2.2.1 Sampling design

206 Following previous research, we divided the study area into 20 km × 20 km equal-area blocks and designed the two-stage
 207 cluster sampling to target fields to visit. We first derived the per-block maize and soybean area fractions from the previous

208 year's crop map, sorted all blocks from the highest to the lowest fraction, and then stratified the ranked blocks into high,
 209 medium and low strata. Following previous studies (King et al., 2017; Song et al., 2017), we selected a simple random sample
 210 of blocks from each stratum as the primary sampling units (PSUs) and selected a simple random sample of $10\text{ m} \times 10\text{ m}$ pixels
 211 in each PSU as the secondary sampling units (SSUs) (Figure 5a) (see Table S2).



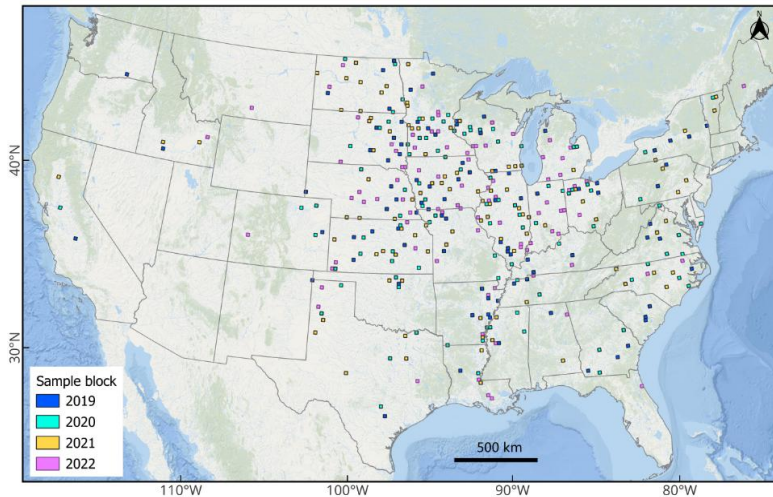
212
 213 **Figure 5: 2022 stratified sampling design for field survey. (a) stratified sampling design. $20\text{ km} \times 20\text{ km}$ equal-area blocks were**
 214 **stratified into high, medium and low strata. (b) crop calendar for maize and soybean over the US. Google Earth imagery is used as**
 215 **background.**

216 2.2.2 Field data collection

217 The typical planting season of the US maize starts in April while soybean planting starts in May; the harvesting season starts
 218 in September and ends in November for maize and in October for soybean (see Figure 5b above). We conducted the field
 219 survey during the peak growing season in July and August. Consistent with previous research (Li et al., 2023; Song et al.
 220 2021a), we collected two types of datasets during the field survey: 1) ground reference data over the probability sample of
 221 SSUs for map evaluation and crop area estimation; and 2) “windshield survey” reference data for model training. These

222 windshield survey data were collected along the driving routes between the SSUs, and were only used to train models for
223 classification and not for validation, whereas the probability sample was exclusively used for validation.

224 For each year from 2019 to 2022, we selected annual probability a separate stratified two-stage cluster sample following the
225 general sampling framework and collected in-season ground data (Figure 6, Table S2-S4).



226
227 **Figure 6: Annual primary sampling unit (PSU) blocks from 2019 to 2022. The ESRI map is used as background.**

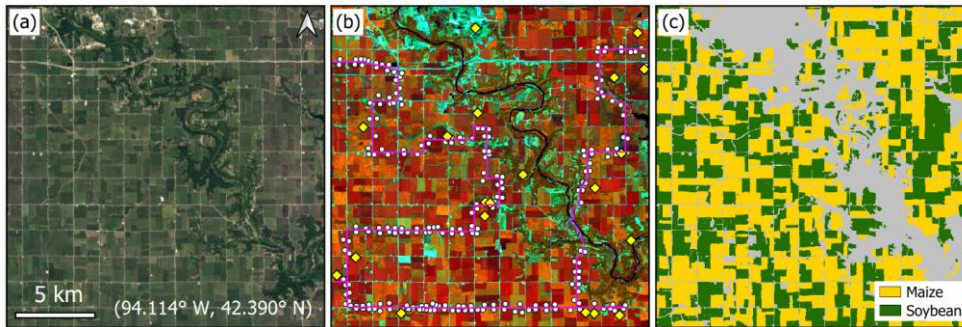
228 2.3 Crop classification

229 We conducted crop classifications in two stages: 1) at the PSU level, we mapped maize and soybean over all the sample PSUs
230 using field data, Sentinel-2 time-series imagery, and decision tree classifiers; and 2) at the national scale, we employed random
231 forest classifiers to map maize and soybean using the PSU-maps as training, multi-temporal metrics derived from Sentinel-2
232 ARD as well as the topographic features derived from TanDEM-X (DLR, 2024) as input. We evaluated the accuracy of the
233 national crop map using the field data over from the SSUs to determine the reference class labels as references.

234 2.3.1 PSU-level crop mapping

235 We processed all available Sentinel-2 data over the PSUs from May 1 to October 31 to produce in-season PSU-level for maize
236 and soybean maps mapping. We trained two decision tree classifiers separately for maize and soybean classification by using
237 all the bands and normalized ratios of any two bands, as well as the “windshield survey” points as training (Figure 7b).
238 Applying the trained models to time-series images, we created a binary maize/non-maize map and a binary soybean/non-

239 soybean map at 10-m resolution for each PSU (Figure 7c). These in-season PSU maps were then pooled as training labels used
240 for national-scale wall-to-wall mapping.



241
242 **Figure 7: An example of primary sampling unit (PSU) block-level crop mapping using field data. (a) a representative sample block**
243 **in Illinois with center coordinates shown on the Google Earth imagery. (b) field data collection in the PSU. The secondary sampling**
244 **units (SSUs) of pixels are shown as yellow diamonds. The “windshield survey” points are shown as white dots. The driving routes**
245 **are shown in pink tracks. (c) PSU-level crop maps.**

246 2.3.2 Wall-to-wall crop classification

247 The multi-temporal metrics derived from the Sentinel-2 ARD were the main input for national mapping. In addition, we
248 downloaded the nominal 12-m TanDEM-X data from the German Aerospace Center (DLR, 2024), and derived 10-m spatial
249 resolution elevation, slope, and aspect using nearest neighbor resampling. These topographic data were combined with the
250 multi-temporal metrics (see Section 2.1.4 above) as inputs for supervised classification. We generated training labels from the
251 10-m maize and soybean PSU maps. We randomly selected 0.2% of maize (soybean) and 0.8% of non-maize (non-soybean)
252 pixels from each PSU as training labels. Conflict classification pixels from the binary maize and soybean maps were excluded
253 in the training dataset.

254 To conduct crop classifications, we employed Random Forest (RF), a widely adopted ensemble machine learning algorithm
255 in remote sensing due to its accuracy, computational efficiency, and robustness to noise (Belgiu and Drăguț, 2016; Breiman,
256 2001). Following the approach detailed in Li et al. (2023), we tailored RF binary classifiers separately for maize (RF-Maize)
257 and soybean (RF-Soybean). The models were fine-tuned using a random search followed by a grid search (Probst et al., 2019),
258 on a randomly selected subset of 1% of the training dataset, and subsequently re-trained with optimal hyperparameters on the
259 entire training dataset (see more technical details in Figure S1, Figure S2 and Table S53).

260 We aggregated the per-pixel class probability layers from RF-Maize and RF-Soybean by selecting the highest probability
261 (maize vs. soybean) and derived the aggregated probability layer and corresponding crop mask layer (see Figure S3 for an
262 example). We then applied a 5×5 pixel kernel opening followed by a 10×10 pixel kernel closing \ominus to eliminate scattered

pixels and fill holes within large homogeneous fields. The kernel sizes were selected based on tests and visual assessments to balance noise removal while preserving fine details. We generated the final maize and soybean map using the combined aggregated probability layers following the area-matching approach reported by Song et al (2017), Song et al. (2021b) and Li et al. (2023).

2.4 Map evaluation

2.4.1 Accuracy assessment

Utilizing the annually field-visited SSUs, we validated the annual maps from 2019 to 2022. Overall accuracy (OA), user's accuracy (UA) and producer's accuracy (PA) with associated uncertainty estimates were estimated using a ratio estimator for two-stage cluster sampling within a stratified design, following good practices (Olofsson et al., 2013; Stehman, 2014). The formulas for accuracy estimation ~~are~~ found in Song et al. (2017, Appendix A.)

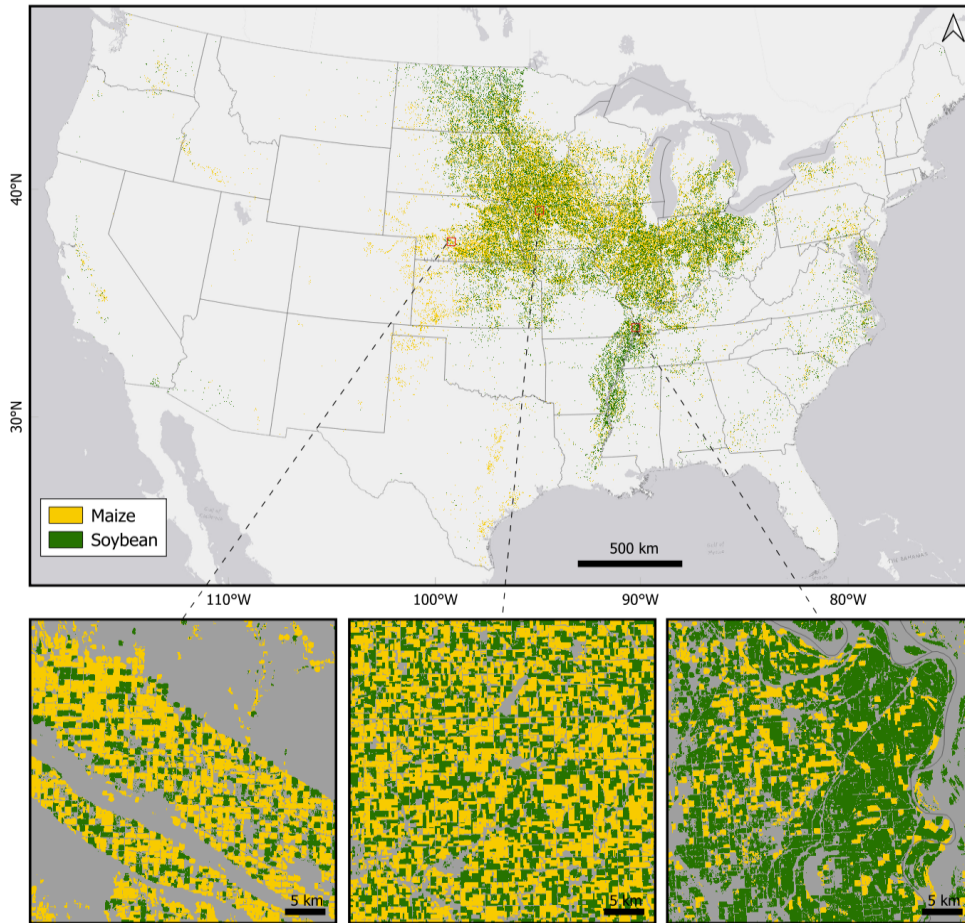
2.4.2 Crop area comparison with official statistics

We derived the pixel-counting-based crop areas for maize and soybean from the annual crop maps, for each year from 2019 to 2022. We compared these crop areas with the official statistical crop areas from the USDA NASS at the county and state levels. We then calculated root-mean-square-difference (RMSD) and r^2 between the mapped crop areas and the statistical areas.

3 Results

3.1 Visual assessment

Our 10-m crop map reveals well-known spatial patterns of maize and soybean cultivation in the United States (Figure 8). The dominant soybean cultivation is shown in the Midwest states, the Great Plains states, the Mississippi Valley and the eastern coast, whereas maize is widely distributed across the country.



283

284

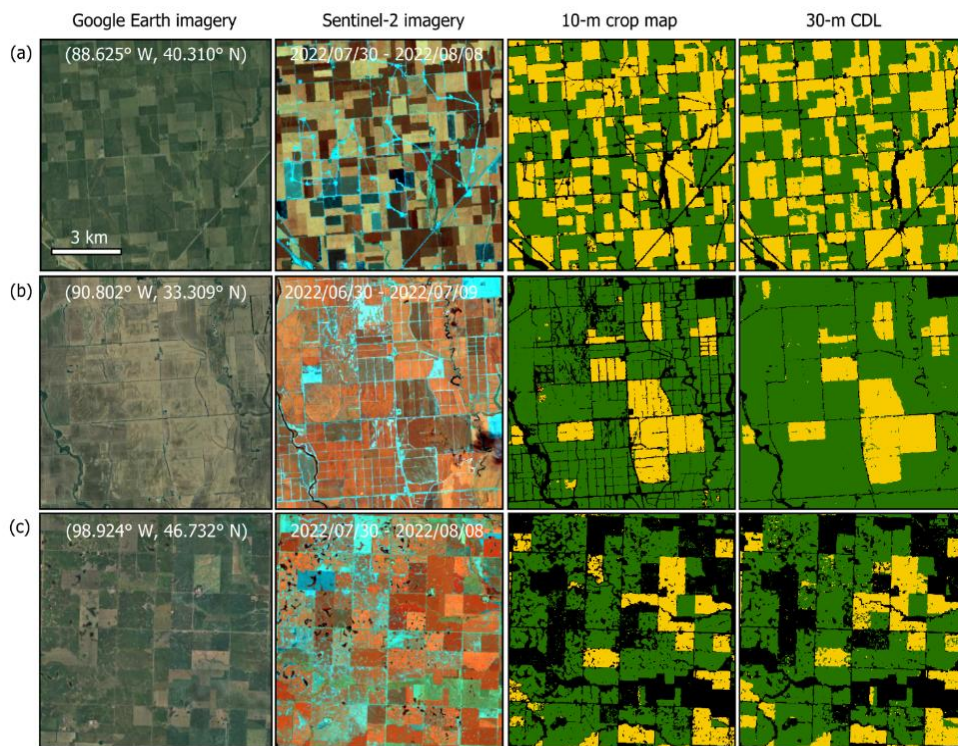
Figure 8: The 10-m maize and soybean map for 2022. The ESRI map is used as background.

285

Specifically, our 10-m crop map delineated more field-scale details compared to the 30-m CDL (Figure 9). Midwest states such as Illinois typically have rectangular crop fields, and our 10-m map generated homogeneous fields with clearer boundaries (Figure 9a). Our map also captured more landscape fragmentation, such as smaller fields with greater crop diversity in the Mississippi Valley (Figure 9b) and the agriculture/wetland mosaic in North Dakota (Figure 9c).

288

289



290
 291 **Figure 9:** Maize and soybean classification in 2022 over selected regions. Rows (a-c) are representative sites in Illinois, Mississippi,
 292 and North Dakota. All panels are displayed at the same scale (10 km × 10 km). The coordinates of the center points are shown on
 293 the Google Earth imagery. The 10-day composite periods are shown on the Sentinel-2 image (R: NIR, G: SWIR1, B: SWIR2).
 294 Maize and soybean are shown in yellow and green colors, respectively.

295 **3.2 Quantitative accuracy assessment**

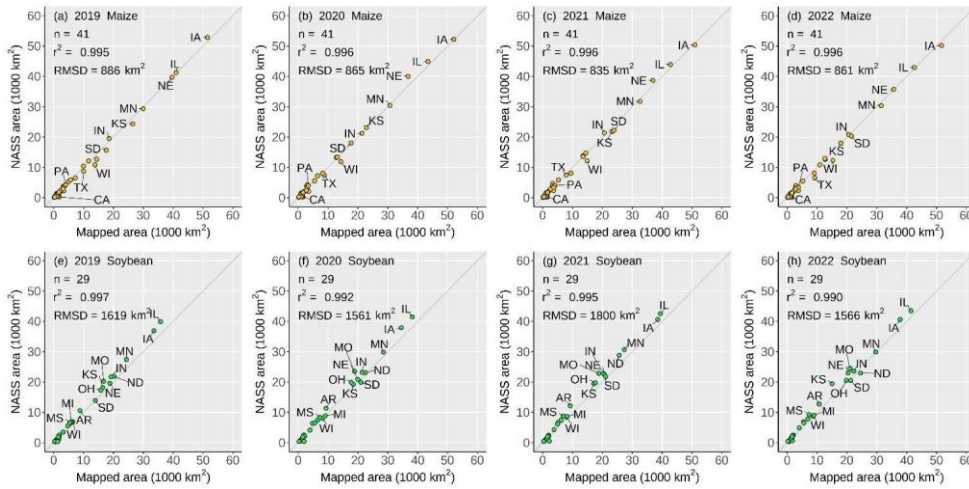
296 We conducted an accuracy assessment for annual maps using the annual SSUs as references (Table 1). All maps achieved OAs
 297 greater than 95% with standard errors less than 1%. UAs and PAs for maize were higher than 91% and 84%, respectively,
 298 while UAs and PAs for soybean were higher than 89% and 82%, respectively.

302
303**Table 1: Accuracy assessment for maize and soybean maps from 2019 to 2022. Cell entries in the confusion matrices represent area proportions. Reference data were derived from probability samples of secondary sampling units (SSUs).**

Year	Class	Reference				Users'	Producers'	Overall
		Maize	Soybean	Others	Total	accuracy % (SE)	accuracy % (SE)	accuracy % (SE)
2019	Maize	0.1111	0.0017	0.0053	0.1181	94.0 (1.5)	85.6 (2.6)	95.4 (0.5)
	Soybean	0.0003	0.0868	0.0056	0.0927	93.7 (1.8)	83.8 (2.4)	
	Others	0.0183	0.0150	0.7558	0.7891	95.8 (0.6)	98.6 (0.3)	
	Total	0.1297	0.1036	0.7667	1			
2020	Maize	0.1073	0.0031	0.0045	0.1149	93.4 (1.6)	91.0 (1.8)	95.9 (0.5)
	Soybean	0.0012	0.0941	0.0086	0.1039	90.6 (1.8)	84.5 (2.7)	
	Others	0.0095	0.0141	0.7576	0.7812	97.0 (0.5)	98.3 (0.3)	
	Total	0.1180	0.1113	0.7707	1			
2021	Maize	0.1021	0.0044	0.0053	0.1118	91.2 (1.8)	92.8 (1.5)	95.3 (0.6)
	Soybean	0.0012	0.0967	0.0109	0.1088	89.3 (2.5)	82.1 (2.5)	
	Others	0.0066	0.0168	0.7560	0.7793	96.8 (0.5)	97.8 (0.4)	
	Total	0.1098	0.1179	0.7723	1			
2022	Maize	0.0884	0.0024	0.0055	0.0963	91.8 (2.0)	84.0 (3.5)	95.3 (0.7)
	Soybean	0.0019	0.0904	0.0095	0.1018	88.8 (4.0)	85.8 (2.5)	
	Others	0.0150	0.0126	0.7744	0.8020	96.6 (0.6)	98.1 (0.6)	
	Total	0.1052	0.1054	0.7894	1			

304 **3.3 Comparison between the crop maps and agricultural statistics**

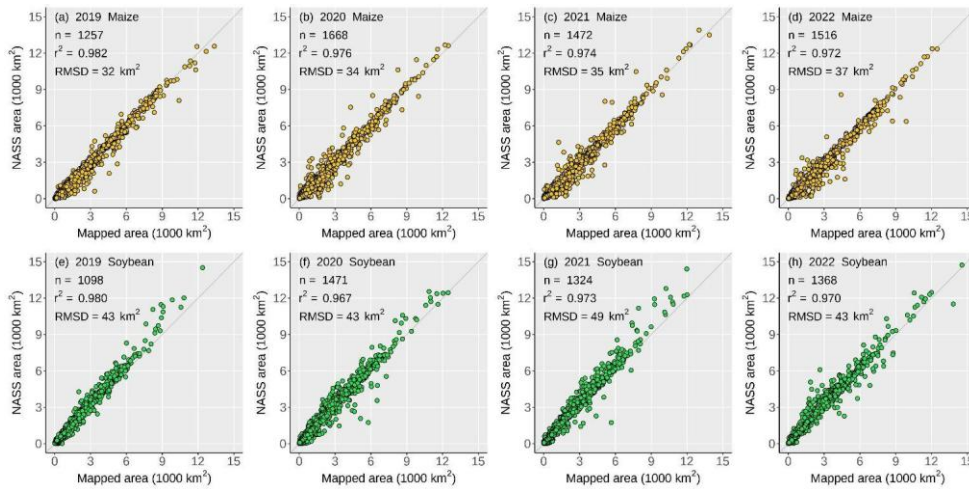
305 We compared our map-based area estimates with agricultural statistics reported by the NASS at state and county scales. The
306 state-level area comparisons between our mapped areas and the NASS statistics showed close agreements, with r^2 greater than
307 0.99 and root-mean-square-difference (RMSDs) less than 900 km² for maize, and RMSDs less than 1,800 km² for soybean
308 (Figure 10). At the county level (Figure 11), our mapped maize and soybean areas also matched the NASS statistics well with
309 r^2 greater than 0.97 and RMSDs between 30 km² and 50 km².



310

311

Figure 10: State-level comparison between mapped maize and soybean areas and NASS statistics.



312

313

Figure 11: County-level comparisons between mapped maize and soybean areas and NASS statistics.

314 **4 Discussion**

315 **4.1 The benefits of 10-m crop maps in mixed pixel reduction**

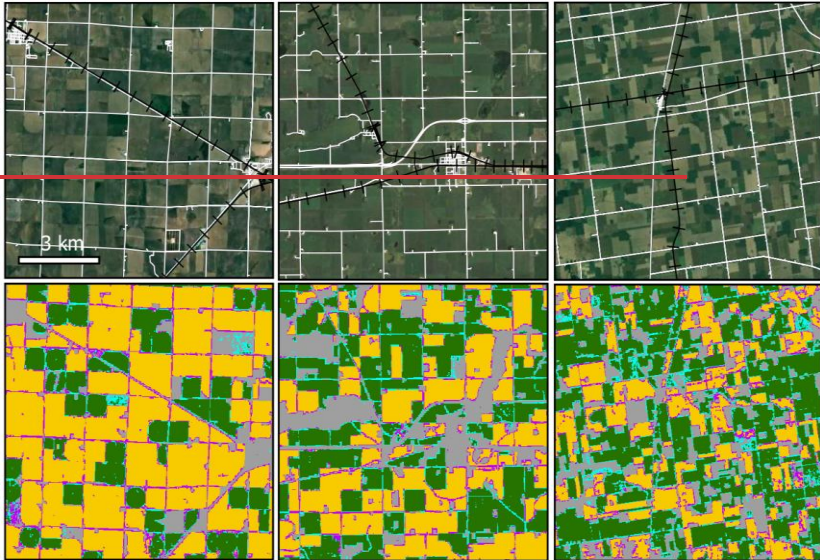
316 Using the 2022 10-m crop map as an example, we conducted a quantitative data analysis to illustrate the benefits of 10-m crop
317 mapping over 30-m mapping. We first removed small fields less than 9 10-m pixels (one 30-m pixel), then spatially aggregated
318 the 10-m map to 30-m resolution and derived the maize and soybean cover fraction for each 30-m pixel. We defined pure
319 pixels as 100% cover and anything below as mixed pixels. We applied a 50% cover threshold to determine the dominant crop
320 type within mixed pixels. Pixels where neither maize nor soybean cover reached 50% were ignored. Rather than assessing
321 accuracies for the aggregated 30-m maps, our objective was to compare the 10-m versus 30-m resolution by quantifying
322 changes in mixed pixels and analyzing the spatial patterns.

323 Unsurprisingly, the aggregated 30-m map showed that pure pixels are clustered in large-size homogeneous fields (Figure 12a).
324 Mixed pixels occurred in small, fragmented fields, on field edges, or along the road networks, where crops coexisted with
325 other land cover (e.g., other crops, pasture, built-up, etc.) (Figure 12b, c). Our 10-m maps showed clear advantages over the
326 30-m CDL in mixed pixel reduction in various landscapes (Figure 13). In North Dakota where numerous fields are fragmented,
327 the 10-m map presents more homogeneous fields and captures within-field patterns of water ponds (Figure 13a); for center-
328 pivot irrigated fields in Nebraska, the 10-m map delineates cleaner circular patterns (Figure 13b); in Appalachian Pennsylvania
329 where many fields are in narrow strips, the 10-m map distinguishes neighboring strip cropping fields better than the 30-m CDL
330 in which the fields are mapped with a large amount of mixed pixels (Figure 13c).

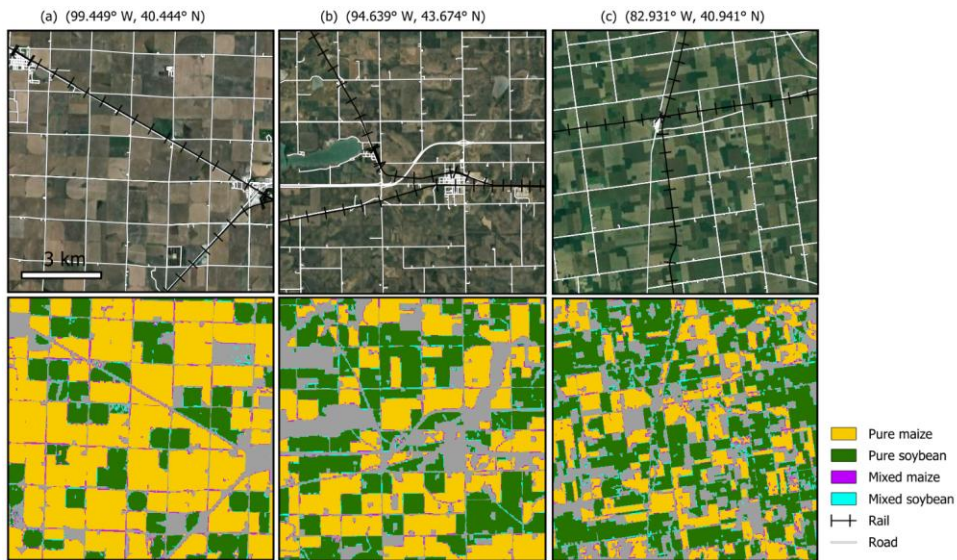
(a) (99.449° W, 40.444° N)

(b) (94.639° W, 43.674° N)

(c) (82.931° W, 40.941° N)



331



332

333

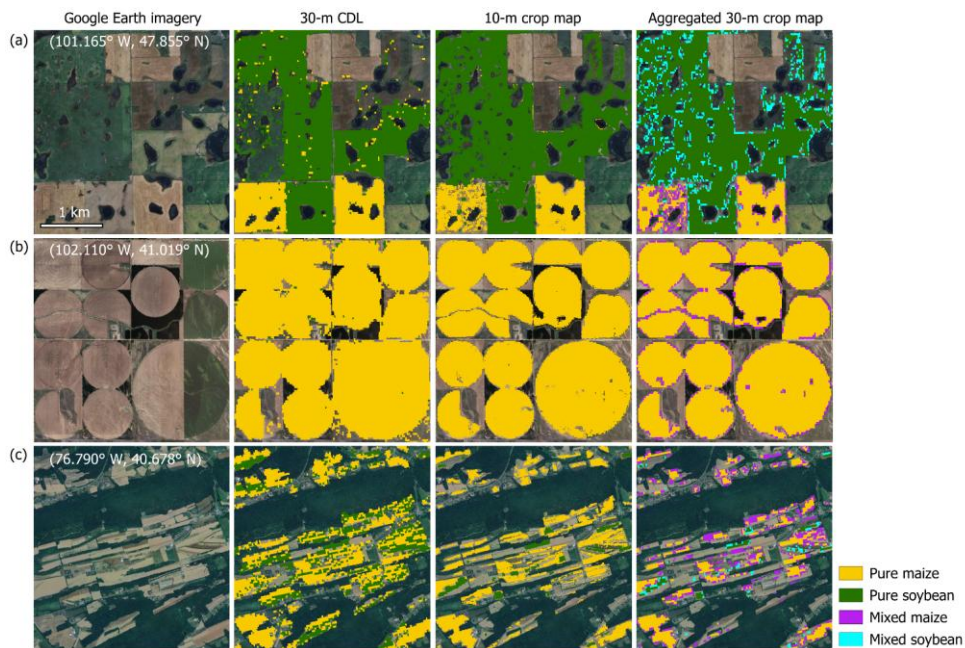
334

335

336

337

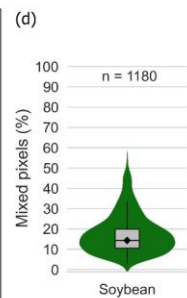
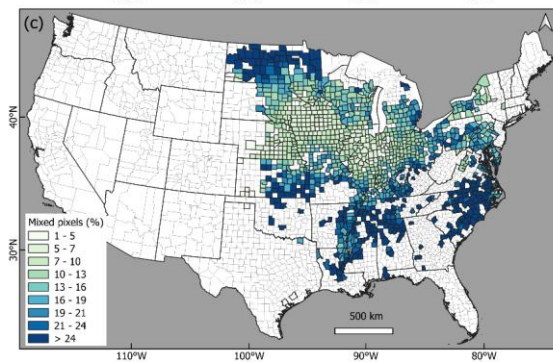
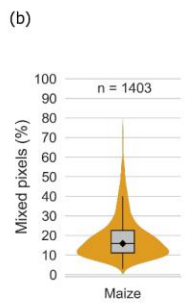
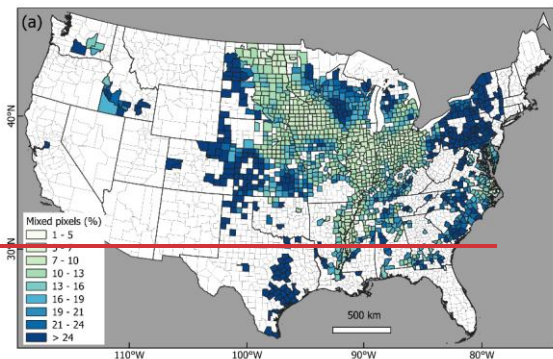
Figure 12: The 2022 aggregated 30-m maize and soybean map overlaid with road and rail networks. Columns (a-c) are selected sites in Nebraska, Minnesota, and Ohio. The 30-m map was derived by spatially aggregating the 10-m map by calculating the fractional cover and categorized as pure pixels with 100% cover or mixed pixels with <100% cover. All panels are displayed at the same scale (10 km × 10 km). The coordinates of the center points are shown on the Google Earth imagery. The rail and road networks are obtained from the US TIGER database.



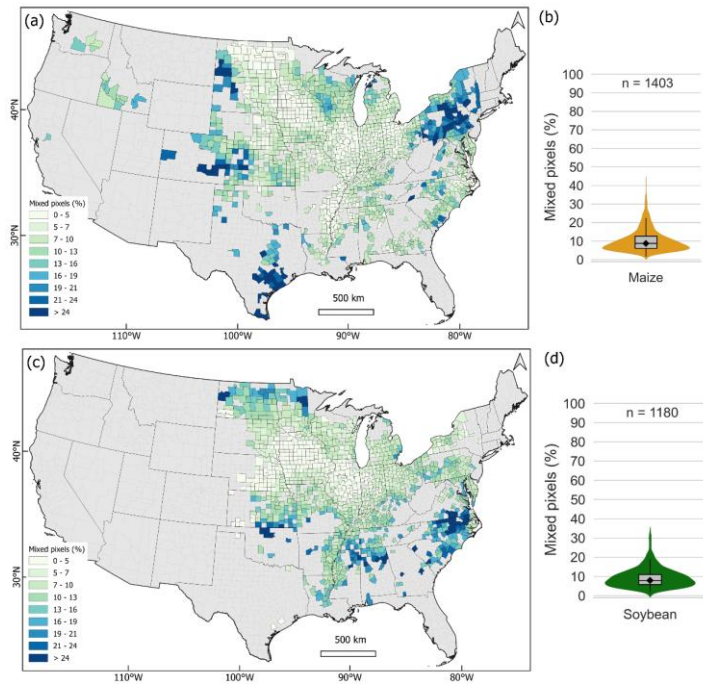
338

339 **Figure 13: The 2022 aggregated 30-m maize and soybean map and CDL show mixed pixels in various landscapes. (a)**
 340 **wetland/agriculture mosaics in North Dakota; (b) center-pivot irrigated fields in Nebraska; (c) strip fields in Pennsylvania. The**
 341 **coordinates of the center points are shown on the Google Earth imagery.**

342 We obtained the percentage of mixed maize and soybean pixels at the county level to examine the spatial distribution of mixed
 343 pixel reduction from 30 m to 10 m (Figure 14). The counties with the highest maize and soybean production, such as those in
 344 Iowa, Illinois, and Nebraska, had the least mixed pixel percentages ranging from 1% to 10%, while counties in the upper
 345 Midwest, the North and South Plains, the northeast and eastern coast had more mixed pixels (Figure 14a, Figure 14c). Overall,
 346 the median percentages of mixed maize and soybean pixels in all counties were ~~148%~~ and ~~169%~~, respectively (Figure 14b, d).
 347 Our results show that increasing the spatial resolution of crop mapping from 30 m to 10 m would reduce the number of mixed
 348 pixels by ~~148-169%~~ at the county scale, and substantially benefit many states outside of the Midwest region.



Formatted: Keep with next



350
351 **Figure 14: The percentages of 30-m mixed maize and soybean pixels at the county level derived from the 10-m map. (a) the spatial**
352 **distribution of mixed maize pixels; (b) the statistical distribution of mixed maize pixels; (c-d) the same as (a-b) but for soybean.**
353 **Counties accounting for 99.9% coverage of the national maize and soybean cultivation derived from the 2022 NASS statistics are**
354 **shown.**

355 We conducted additional analysis by comparing our aggregated 30-m map with the 30-m CDL for the maize and soybean
356 classes. We applied a 50% threshold to convert our aggregated 30-m map to binary maize and soybean maps and conducted a
357 per-pixel comparison. We then aggregated the per-pixel results to the county level based on the ratio of the difference of maize
358 or soybean pixels between our map and CDL divided by maize or soybean pixels in CDL. Positive values indicate more maize
359 or soybean pixels in our map, whereas negative values indicate more pixels in CDL (Figure 15). In several regions, our map
360 presented more maize pixels, such as in northern Texas and southern Louisiana (Figure 15a), and more soybean pixels, such
361 as in western North Dakota and Georgia (Figure 15c). In general, CDL reported more maize and soybean pixels in most
362 counties compared to our aggregated 30-m map (Figure 15b, d), which is likely due to the exclusion of 10-m maize and soybean
363 pixels below the 50% threshold during aggregation.

Formatted: Font: 10 pt, Not Bold, Font color: Auto

Formatted: Font color: Auto

Formatted: Font: 10 pt, Not Bold, Font color: Auto

Formatted: Font color: Auto

Formatted: Font: 10 pt, Not Bold, Font color: Auto

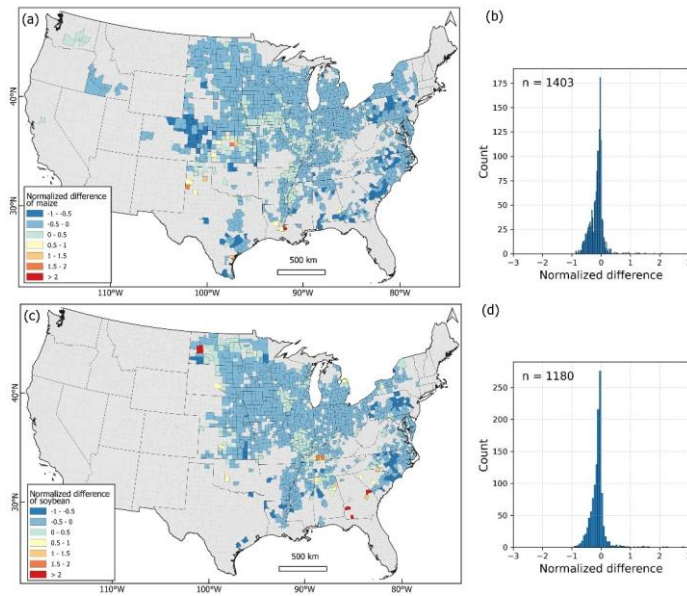
Formatted: Font: 10 pt, Not Bold, Font color: Auto

Formatted: Font color: Auto

Formatted: Font: 10 pt, Not Bold, Font color: Auto

Formatted: Font: 10 pt, Not Bold, Font color: Auto

Formatted: Font color: Auto

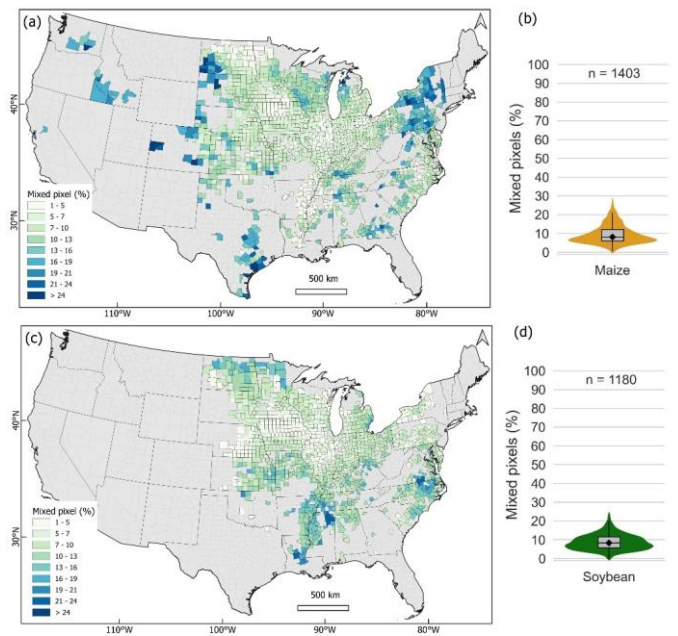


365 **Figure 15: Comparison between our aggregated 30-m map with the 2022 30-m CDL at the county level. (a) normalized difference of**
 366 **maize pixel; (b) histogram of the normalized difference of maize pixel; (c-d) the same as (a-b) but for soybean. Counties accounting**
 367 **for 99.9% coverage of the national maize and soybean cultivation derived from the 2022 NASS statistics are shown.**

368 To estimate the number of mixed pixels that might be reduced by improving the CDL's spatial resolution from 30 m to 10 m,
 369 we overlaid the 2022 30-m CDL on our 30-m fractional cover map, and computed the number and proportion of CDL maize
 370 and soybean pixels that were mixed pixels at the county level (Figure 16). The mixed pixel derived from CDL showed similar
 371 spatial distribution patterns to results derived from the aggregated 30-m map (see Figure 14 above). The median percentage of
 372 mixed pixels across all counties for both maize and soybean was 8% (Figure 16b, d), which is close to the values of 8% (9%
 373 for soybean) derived from our aggregated 30-m map (see Figure 14 above). These consistent mixed pixel estimates from our
 374 map and the CDL indicate substantial benefits of 10-m crop maps in reducing mixed pixels over existing 30-m products,
 375 especially for regions outside of Midwest, as illustrated in our analyses.

Formatted: Keep with next

Formatted: Font color: Auto



377 **Figure 16: The percentages of 30-m mixed maize and soybean pixels at the county level by comparing our aggregated 30-m map and**
 378 **the 2022 30-m CDL. (a) the spatial distribution of mixed maize pixels; (b) the statistical distribution of mixed maize pixels; (c-d) the**
 379 **same as (a-b) but for soybean. Counties accounting for 99.9% coverage of the national maize and soybean cultivation derived from**
 380 **the 2022 NASS statistics are shown.**

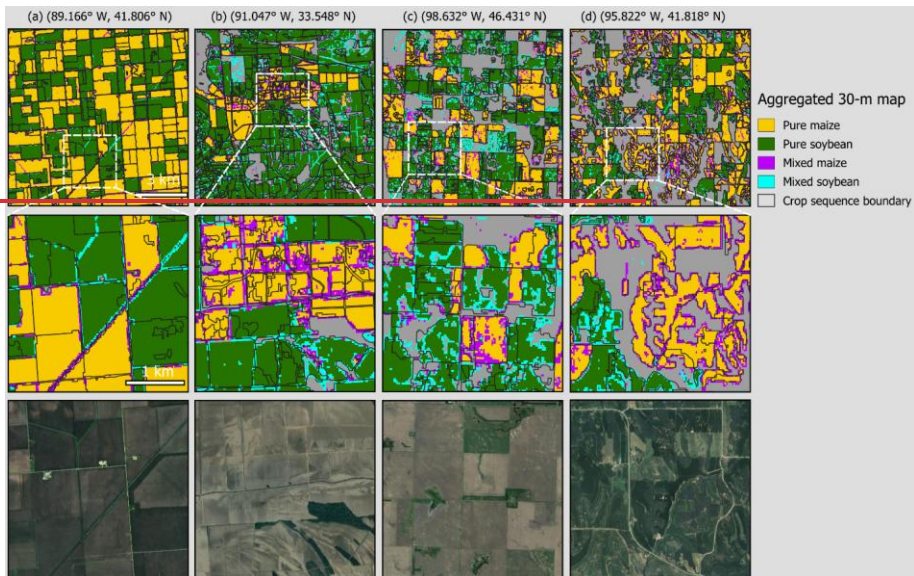
381 **4.2 The potential of 10-m crop maps in finer-scale agricultural monitoring**

382 Higher-resolution crop maps have great potential to facilitate remote-sensing-based agricultural applications at finer scales.
 383 For example, the Crop Sequence Boundaries (CSB), which delineate polygons of homogeneous cropping sequences with 8-
 384 year moving windows, have been developed based on the CDL by the USDA (Hunt et al., 2023). The 30-m CDL was resampled
 385 to 10-m resolution to improve the masking of road networks as the roads and rails in rural areas are typically less than 30 m in
 386 width. Consequently, the resampled 10-m maps may delineate inaccurate field boundaries due to mixed pixels (Figure 15Figure
 387 17). The CSB delineated large homogeneous fields well (Figure 17aFigure 15a) but showed more fragments when
 388 encountering within-field cropping variations (Figure 15Figure 17b). The misalignments between the delineated field edges
 389 and pixel boundaries are extensive in heterogeneous landscapes and small fields (Figure 15Figure 17c, d), and thus the
 390 polygon-based crop acreage derived from CSB layers may be biased. Alternatively, using originally produced higher-

Formatted: Keep with next

Formatted: Caption, Space After: 0 pt, Border: Top: (No border), Bottom: (No border), Left: (No border), Right: (No border), Between : (No border)

391 resolution (e.g., 10-m) maps can yield more accurate field delineation, cropping sequences, and crop area estimates with
392 smaller uncertainties (Duveiller and Defourny, 2010; Ozdogan and Woodcock, 2006; Yan and Roy, 2014).





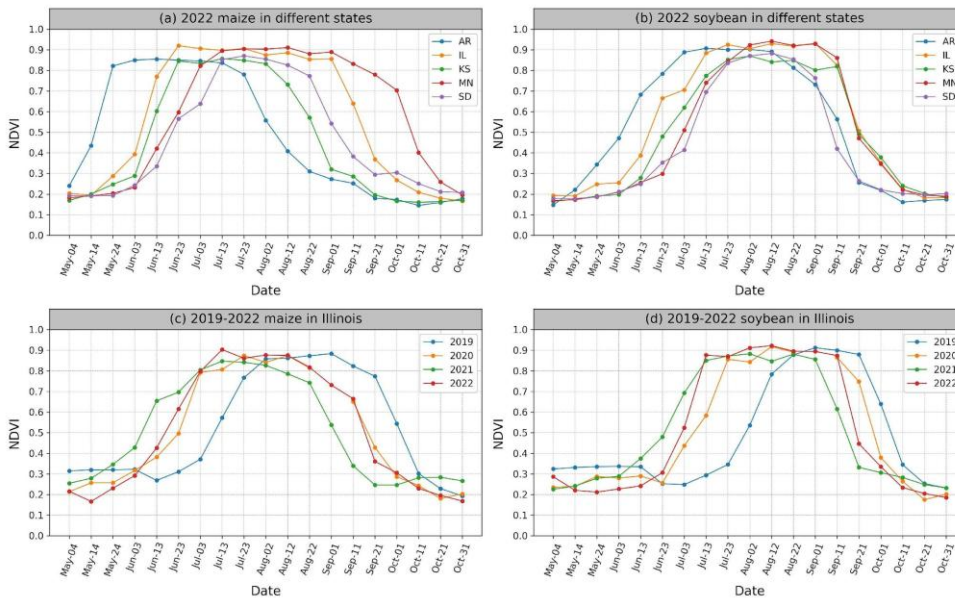
394
395 **Figure 17: The aggregated 30-m maize and soybean map overlaid with Crop Sequence Boundaries. Columns (a-d) are selected sites**
396 **in Illinois, Mississippi, North Dakota, and Iowa. All panels are displayed at the same scale (10 km × 10 km). The coordinates of the**
397 **center points are shown. The 2015-2022 Crop Sequence Boundaries are obtained from the USDA NASS.**

398 With higher-resolution satellite imagery available from continuous observations (e.g., Sentinel-1 and Sentinel-2) and upcoming
399 missions (e.g., Landsat Next, NASA-ISRO SAR Mission (NISAR)), we anticipate that 10-m crop maps will play a more
400 critical role in agricultural monitoring from the field to global scales.

401 **4.3 The robustness of temporal metrics for annual crop map production**

402 Stacking satellite-derived time-series maps is one of the most common practices to investigate long-term agriculture-related
403 land cover and land use change, such as cropping history (Blickensdörfer et al., 2022; Johnson, 2019), crop and cropland
404 expansion (Lark et al., 2020; Potapov et al., 2021a; Song et al., 2021b; Zalles et al., 2019), and cropland intensification (Kehoe
405 et al., 2017; Marin et al., 2022). However, in large-extent countries such as the US, the spatiotemporal consistency in multi-
406 year crop classifications can be impacted by both intra-annual and interannual variations in crop phenology (Figure 18
407 Figure 16). For example, the 2022 NDVI time series for maize and soybean showed noticeably different crop progress across the
408 CONUS (Figure 16 Figure 18a, Figure 16 Figure 18b). In Arkansas, maize growth peaked in mid-May and started senescence
409 in early August, whereas maize in the Midwest states was at early growing stages in mid-May and at the peak growing season
410 in early August. Soybean also showed noticeable disparities in crop progress across the US states. On the other hand,

411 interannual phenological shifts also impede the classification consistency (Figure 16Figure 18c, Figure 16Figure 18d). In
 412 Illinois, similar NDVI profiles between 2020 and 2022 suggested overall consistent growing progress, while the patterns in
 413 2019 and 2021 showed higher interannual variations. In 2021, Illinois experienced an earlier planting pace for maize and
 414 soybean partly due to the favorable spring weather conditions and soybean varieties adapted to early plantation (Nafziger,
 415 2024). In 2019, crop phenology shifted substantially as a result of planting delays caused by extremely heavy precipitation in
 416 the spring (Manoochehr et al., 2021). Consequently, at the state level in Illinois, maize was planted at only 24% compared to
 417 the previous year's 95% and the five-year average of 49% by the end of May 2019; soybean was planted at 9% compared to
 418 the previous year's 79% and the five-year average of 51% (NASS CPR, 2024).



419
 420 **Figure 18: NDVI time series for maize and soybean from representative sites. (a) 2022 maize NDVI in Arkansas (AR), Illinois (IL),**
 421 **Kansas (KS), Minnesota (MN), South Dakota (SD); (b) the same as (a) but for soybean; (c) 2019-2022 interannual NDVI variations**
 422 **for maize in Illinois; (d) the same as (c) but for soybean. The details about the sites are shown in Figure S43 and Table S64.**

423 Utilizing the multi-temporal metrics to relatively normalize crop phenological variations, our approach can be applied to
 424 generate annual crop maps over large areas, as also illustrated for South America in Song et al. (2021b). Our four-year sampling
 425 designs generated large field samples, allowing us to collect representative training data from various growing conditions and
 426 geographical regions. Our workflow generated consistently accurate maize and soybean maps over the entire CONUS, from

427 2019 to 2022. The map accuracies for 2019 (an abnormally wet year), and 2020 and 2021 (both years with normal weather)
428 are consistent with those of 2022 (see Table 1 above).

429 5 Data availability

430 The annual 10-m maize and soybean maps over the CONUS from 2019 to 2022 are openly accessible at the website of the
431 Global Land Analysis and Discovery (GLAD) team at the University of Maryland ([https://glad.umd.edu/dataset/mapping-](https://glad.umd.edu/dataset/mapping-crops-10-m-resolution-united-states)
432 [crops-10-m-resolution-united-states](https://glad.umd.edu/projects/mapping-crops-10-m-resolution-united-states)<https://glad.umd.edu/projects/mapping-crops-10-m-resolution-united-states>). The dataset
433 is also available at <https://doi.org/10.6084/m9.figshare.28934993.v2><https://doi.org/10.6084/m9.figshare.28934993.v1> (Li et
434 al., 2025). The dataset includes a set of GeoTIFF images in the ESPG:4236 spatial reference system. The values 0, 1, 2, 255
435 represent ~~other~~, maize, ~~and~~ soybean, ~~and no data~~, respectively. ~~External D~~ata used in this study are openly accessible online:
436 1) the Sentinel-2 data were downloaded from Google Cloud Platform
437 (<https://console.cloud.google.com/marketplace/product/esa-public-data/sentinel2>); 2) the Cropland Data Layer were
438 downloaded from the US Department of Agriculture (USDA) National Agricultural Statistics Service (NASS)
439 (https://www.nass.usda.gov/Research_and_Science/Cropland/Release/index.php); 3) the TanDEM-X was downloaded from
440 the German Aerospace Center (<https://tandemx-science.dlr.de>); 4) the agricultural statistics for CONUS were retrieved from
441 the USDA NASS (https://www.nass.usda.gov/Quick_Stats/index.php); 5) the Crop Sequence Boundaries were derived from
442 the USDA NASS (https://www.nass.usda.gov/Research_and_Science/Crop-Sequence-Boundaries/index.php); 6) the road and
443 rail networks were downloaded from the US TIGER database ([https://www.census.gov/geographies/mapping-files/time-](https://www.census.gov/geographies/mapping-files/time-series/geo/tiger-line-file.html)
444 [series/geo/tiger-line-file.html](https://www.census.gov/geographies/mapping-files/time-series/geo/tiger-line-file.html)).

445 6 Conclusions

446 Crop maps at 10-m spatial resolution bring substantial benefits for agricultural applications compared to 30-m products for
447 smallholder as well as industrial agricultural countries. In this study, we developed ~~the first openly available~~ 10-m maize and
448 soybean maps over the Contiguous US (CONUS) from 2019 to 2022, using all available Sentinel-2 observations and field
449 surveys, with overall accuracies consistently greater than 95%. We explicitly examined the benefits of improving the spatial
450 resolution from 30 m to 10 m by quantifying the reduction in mixed pixels. Our analysis showed that, across all counties in
451 the US, the 10-m maps ~~could reduced~~ mixed pixels by a median of ~~148~~% for maize and ~~169~~% for soybean compared to the
452 aggregated 30-m maps, with most mixed pixels occurring along field edges, road networks, and in heterogeneous fields. Our
453 workflow ~~can generate~~d annual maps with consistency across space and over time. Our 10-m crop maps ~~were could be~~ produced
454 at the end of the growing season, around 3~4 months earlier than the official 30-m Cropland Data Layer. As more Sentinel-2-
455 like data become accessible from current observations and planned missions such as Landsat Next, 10-m crop maps presented

456 in this study will greatly benefit agricultural applications including field boundary extraction, crop sequence delineation, crop
457 condition monitoring, precision fertilization and irrigation, from field to global scales.

458 **Author contributions**

459 **HL:** Software, Formal analysis, Investigation, Writing - Original Draft, Writing - Review & Editing, Visualization. **XPS:**
460 Conceptualization, Methodology, Software, Formal analysis, Investigation, Writing - Original Draft, Writing - Review &
461 Editing, Supervision, Project administration, Resources, Funding acquisition. **BA:** Formal analysis, Investigation. **JP:** Formal
462 analysis, Investigation, Data Curation. **AL:** Formal analysis, Investigation. **AP:** Formal analysis, Investigation, Data Curation,
463 Writing - Review & Editing. **AB:** Investigation. **PP:** Methodology, Investigation, Software, Writing - Review & Editing. **AK:**
464 Methodology, Investigation, Writing - Review & Editing. **VZ:** Methodology, Investigation. **AHS:** Investigation. **SMJ:**
465 Investigation, Writing - Review & Editing. **AHP:** Investigation. **COD:** Investigation. **XL:** Investigation, Writing - Review &
466 Editing. **TK:** Investigation, Writing - Review & Editing. **ZS:** Investigation. **ST:** Investigation. **EB:** Investigation. **HKK:**
467 Investigation. **AK:** Investigation. **SVS:** Methodology, Writing - Review & Editing. **MCH:** Conceptualization, Methodology,
468 Resources, Investigation, Funding Acquisition.

469 **Competing interests**

470 The authors declare that they have no known competing financial interests or personal relationships that could have appeared
471 to influence the work reported in this paper.

472 **Financial support**

473 This research is supported by the Bezos Earth Fund, Google Academic Research Awards, NASA Land-Cover and Land-Use
474 Change Program, NASA Acres Program, and the University of Maryland. The authors acknowledge the University of
475 Maryland supercomputing resources (<http://hpcc.umd.edu>) made available for conducting the research reported in this paper.

476 **References**

477 de Abelleira, D., Veron, S., Banchemo, S., Mosciaro, M. J., Propato, T., Ferraina, A., Taffarel, M. C. G., Dacunto, L., Franzoni,
478 A., and Volante, J.: First large extent and high resolution cropland and crop type map of Argentina, in: 2020 IEEE Latin
479 American GRSS & ISPRS Remote Sensing Conference (LAGIRS), 392–396,
480 <https://doi.org/10.1109/LAGIRS48042.2020.9165610>, 2020.

481 Alami Machichi, M., mansouri, Ioubna E., imani, yasmina, Bourja, O., Lahlou, O., Zennayi, Y., Bourzeix, F., Hanadé
482 Houmma, I., and Hadria, R.: Crop mapping using supervised machine learning and deep learning: a systematic literature
483 review, *International Journal of Remote Sensing*, 44, 2717–2753, <https://doi.org/10.1080/01431161.2023.2205984>, 2023.

484 Badhwar, G. D.: Classification of corn and soybeans using multitemporal thematic mapper data, *Remote Sensing of*
485 *Environment*, 16, 175–181, [https://doi.org/10.1016/0034-4257\(84\)90061-0](https://doi.org/10.1016/0034-4257(84)90061-0), 1984.

486 Belgiu, M. and Drăguț, L.: Random forest in remote sensing: A review of applications and future directions, *ISPRS Journal of*
487 *Photogrammetry and Remote Sensing*, 114, 24–31, <https://doi.org/10.1016/j.isprsjprs.2016.01.011>, 2016.

488 Blickensdörfer, L., Schwieder, M., Pflugmacher, D., Nendel, C., Erasmi, S., and Hostert, P.: Mapping of crop types and crop
489 sequences with combined time series of Sentinel-1, Sentinel-2 and Landsat 8 data for Germany, *Remote Sensing of*
490 *Environment*, 269, 112831, <https://doi.org/10.1016/j.rse.2021.112831>, 2022.

491 Bolton, D. K. and Friedl, M. A.: Forecasting crop yield using remotely sensed vegetation indices and crop phenology metrics,
492 *Agricultural and Forest Meteorology*, 173, 74–84, <https://doi.org/10.1016/j.agrformet.2013.01.007>, 2013.

493 Boryan, C., Yang, Z., Mueller, R., and Craig, M.: Monitoring US agriculture: the US Department of Agriculture, National
494 Agricultural Statistics Service, Cropland Data Layer Program, Geocarto International, 26, 341–358,
495 <https://doi.org/10.1080/10106049.2011.562309>, 2011.

496 Breiman, L.: Random forests, *Machine Learning*, 45, 5–32, <https://doi.org/10.1023/a:1010933404324>, 2001.

497 CROME, Crop Map of England: <https://environment.data.gov.uk/dataset/cc389fe9-f026-4b20-a80f-f424ee833ea6>, last access:
498 28 May 2024.

499 Defourny, P., Bontemps, S., Bellemans, N., Cara, C., Dedieu, G., Guzzonato, E., Hagolle, O., Inglada, J., Nicola, L., Rabaute,
500 T., Savinaud, M., Udroui, C., Valero, S., Bégué, A., Dejoux, J.-F., El Harti, A., Ezzahar, J., Kussul, N., Labbassi, K.,
501 Lebourgeois, V., Miao, Z., Newby, T., Nyamugama, A., Salh, N., Shelestov, A., Simonneaux, V., Traore, P. S., Traore, S. S.,
502 and Koetz, B.: Near real-time agriculture monitoring at national scale at parcel resolution: Performance assessment of the
503 Sen2-Agri automated system in various cropping systems around the world, *Remote Sensing of Environment*, 221, 551–568,
504 <https://doi.org/10.1016/j.rse.2018.11.007>, 2019.

505 DeFries, R., Hansen, M., and Townshend, J.: Global discrimination of land cover types from metrics derived from AVHRR
506 pathfinder data, *Remote Sensing of Environment*, 54, 209–222, [https://doi.org/10.1016/0034-4257\(95\)00142-5](https://doi.org/10.1016/0034-4257(95)00142-5), 1995.

507 Deines, J. M., Swatantran, A., Ye, D., Myers, B., Archontoulis, S., and Lobell, D. B.: Field-scale dynamics of planting dates
508 in the US Corn Belt from 2000 to 2020, *Remote Sensing of Environment*, 291, <https://doi.org/10.1016/j.rse.2023.113551>,
509 2023.

510 DLR, TanDEM-X - Digital Elevation Model (DEM) - Global, 12m: <https://tandemx-science.dlr.de/>, last access: 20 June 2024.

511 Dong, J., Xiao, X., Menarguez, M. A., Zhang, G., Qin, Y., Thau, D., Biradar, C., and Moore, B.: Mapping paddy rice planting
512 area in northeastern Asia with Landsat 8 images, phenology-based algorithm and Google Earth Engine, *Remote Sensing of*
513 *Environment*, 185, 142–154, <https://doi.org/10.1016/j.rse.2016.02.016>, 2016.

514 Duveiller, G. and Defourny, P.: A conceptual framework to define the spatial resolution requirements for agricultural
515 monitoring using remote sensing, *Remote Sensing of Environment*, 114, <https://doi.org/10.1016/j.rse.2010.06.001>, 2010.

516 EU, 2024. The High Resolution Layer Crop Types (CTY). EEA geospatial data catalogue. URL
517 <https://sdi.eea.europa.eu/catalogue/srv/api/records/9db29b07-5968-4ce0-8351-1e356b3d7d47>, last access: 21 November
518 2025.

519 ESA, Monitoring crop health across the Netherlands:
520 [https://www.esa.int/Applications/Observing_the_Earth/Copernicus/Sentinel-](https://www.esa.int/Applications/Observing_the_Earth/Copernicus/Sentinel-1/Monitoring_crop_health_across_the_Netherlands)
521 [1/Monitoring_crop_health_across_the_Netherlands](https://www.esa.int/Applications/Observing_the_Earth/Copernicus/Sentinel-1/Monitoring_crop_health_across_the_Netherlands), last access: 20 June 2024.

522 Escobar, N., Tizado, E. J., zu Ermgassen, E. K. H. J., Löfgren, P., Börner, J., and Godar, J.: Spatially-explicit footprints of
523 agricultural commodities: Mapping carbon emissions embodied in Brazil's soy exports, *Global Environmental Change*, 62,
524 102067, <https://doi.org/10.1016/j.gloenvcha.2020.102067>, 2020.

525 Fisette, T., Rollin, P., Aly, Z., Campbell, L., Daneshfar, B., Filyer, P., Smith, A., Davidson, A., Shang, J., and Jarvis, I.: AAFC
526 annual crop inventory, 2013 Second International Conference on Agro-Geoinformatics (Agro-Geoinformatics), 270–274,
527 <https://doi.org/10.1109/Argo-Geoinformatics.2013.6621920>, 2013.

528 Foerster, S., Kaden, K., Foerster, M., and Itzerott, S.: Crop type mapping using spectral–temporal profiles and phenological
529 information, *Computers and Electronics in Agriculture*, 89, 30–40, <https://doi.org/10.1016/j.compag.2012.07.015>, 2012.

530 Frantz, D., Haß, E., Uhl, A., Stoffels, J., and Hill, J.: Improvement of the Fmask algorithm for Sentinel-2 images: Separating
531 clouds from bright surfaces based on parallax effects, *Remote Sensing of Environment*, 215, 471–481,
532 <https://doi.org/10.1016/j.rse.2018.04.046>, 2018.

533 Fritz, S., See, L., McCallum, I., You, L., Bun, A., Moltchanova, E., Duerauer, M., Albrecht, F., Schill, C., Perger, C., Havlik,
534 P., Mosnier, A., Thornton, P., Wood-Sichra, U., Herrero, M., Becker-Reshef, I., Justice, C., Hansen, M., Gong, P., Abdel Aziz,
535 S., Cipriani, A., Cumani, R., Cecchi, G., Conchedda, G., Ferreira, S., Gomez, A., Haffani, M., Kayitakire, F., Malanding, J.,
536 Mueller, R., Newby, T., Nonguierma, A., Olusegun, A., Ortner, S., Rajak, D. R., Rocha, J., Schepaschenko, D.,
537 Schepaschenko, M., Terekhov, A., Tiangwa, A., Vancutsem, C., Vintrou, E., Wenbin, W., van der Velde, M., Dunwoody, A.,
538 Kraxner, F., and Obersteiner, M.: Mapping global cropland and field size, *Global Change Biology*, 21, 1980–92,
539 <https://doi.org/10.1111/gcb.12838>, 2015.

540 Gao, F., Anderson, M. C., Zhang, X., Yang, Z., Alfieri, J. G., Kustas, W. P., Mueller, R., Johnson, D. M., and Prueger, J. H.:
541 Toward mapping crop progress at field scales through fusion of Landsat and MODIS imagery, *Remote Sensing of*
542 *Environment*, 188, 9–25, <https://doi.org/10.1016/j.rse.2016.11.004>, 2017.

543 Ghassemi, B., Dujakovic, A., Zóltak, M., Immitzer, M., Atzberger, C., and Vuolo, F.: Designing a European-wide crop type
544 mapping approach based on machine learning algorithms using LUCAS field survey and Sentinel-2 data, *Remote Sensing*, 14,
545 <https://doi.org/10.3390/rs14030541>, 2022.

546 Griffiths, P., Nendel, C., and Hostert, P.: Intra-annual reflectance composites from Sentinel-2 and Landsat for national-scale
547 crop and land cover mapping, *Remote Sensing of Environment*, 220, 135–151, <https://doi.org/10.1016/j.rse.2018.10.031>, 2019.

548 Han, J., Zhang, Z., Luo, Y., Cao, J., Zhang, L., Zhang, J., and Li, Z.: The RapeseedMap10 database: annual maps of rapeseed
549 at a spatial resolution of 10 m based on multi-source data, *Earth System Science Data*, 13, 2857–2874,
550 <https://doi.org/10.5194/essd-13-2857-2021>, 2021.

551 Hansen, M. C., Potapov, P. V., Moore, R., Hancher, M., Turbanova, S. A., Tyukavina, A., Thau, D., Stehman, S. V., Goetz,
552 S. J., Loveland, T. R., Kommareddy, A., Egorov, A., Chini, L., Justice, C. O., and Townshend, J. R.: High-resolution global
553 maps of 21st-century forest cover change, *Science*, 342, 850–3, <https://doi.org/10.1126/science.1244693>, 2013.

554 Huang, Y., Qiu, B., Yang, P., Wu, W., Chen, X., Zhu, X., Xu, S., Wang, L., Dong, Z., Zhang, J., Berry, J., Tang, Z., Tan, J.,
555 Duan, D., Peng, Y., Lin, D., Cheng, F., Liang, J., Huang, H., and Chen, C.: National-scale 10 m annual maize maps for China
556 and the contiguous United States using a robust index from Sentinel-2 time series, *Computers and Electronics in Agriculture*,
557 221, 109018, <https://doi.org/10.1016/j.compag.2024.109018>, 2024.

558 Hunt, K. A., Abernethy, J., Bowman, M., Wallander, S., and Williams, R.: Crop Sequence Boundaries (CSB): Delineated
559 fields using remotely sensed crop rotations, USDA-NASS, Washington, DC, USA, 2023.

560 Immitzer, M., Vuolo, F., and Atzberger, C.: First experience with Sentinel-2 data for crop and tree species classifications in
561 Central Europe, *Remote Sensing*, 8, 166, <https://doi.org/10.3390/rs8030166>, 2016.

562 Inglada, J., Arias, M., Tardy, B., Hagolle, O., Valero, S., Morin, D., Dedieu, G., Sepulcre, G., Bontemps, S., Defourny, P., and
563 Koetz, B.: Assessment of an operational system for crop type map production using high temporal and spatial resolution
564 satellite optical imagery, *Remote Sensing*, 7, 12356–12379, <https://doi.org/10.3390/rs70912356>, 2015.

565 Johnson, D. M.: Using the Landsat archive to map crop cover history across the United States, *Remote Sensing of Environment*,
566 232, 111286, <https://doi.org/10.1016/j.rse.2019.111286>, 2019.

567 Johnson, D. M. and Mueller, R.: Pre- and within-season crop type classification trained with archival land cover information,
568 *Remote Sensing of Environment*, 264, <https://doi.org/10.1016/j.rse.2021.112576>, 2021.

569 Joshi, A., Pradhan, B., Gite, S., and Chakraborty, S.: Remote-sensing data and deep-learning techniques in crop mapping and
570 yield prediction: A systematic review, *Remote Sensing*, 15, 2014, <https://doi.org/10.3390/rs15082014>, 2023.

571 Kehoe, L., Romero-Munoz, A., Polaina, E., Estes, L., Kreft, H., and Kuemmerle, T.: Biodiversity at risk under future cropland
572 expansion and intensification, *Nature Ecology & Evolution*, 1, 1129–1135, <https://doi.org/10.1038/s41559-017-0234-3>, 2017.

573 Kerner, H. R., Sahajpal, R., Pai, D. B., Skakun, S., Puricelli, E., Hosseini, M., Meyer, S., and Becker-Reshef, I.: Phenological
574 normalization can improve in-season classification of maize and soybean: A case study in the central US Corn Belt, *Science
575 of Remote Sensing*, <https://doi.org/10.1016/j.srs.2022.100059>, 2022.

576 Khan, A., Hansen, M. C., Potapov, P., Stehman, S. V., and Chatta, A. A.: Landsat-based wheat mapping in the heterogeneous
577 cropping system of Punjab, Pakistan, *International Journal of Remote Sensing*, 37, 1391–1410,
578 <https://doi.org/10.1080/01431161.2016.1151572>, 2016.

579 Khan, A., Hansen, M., Potapov, P., Adusei, B., Pickens, A., Krylov, A., and Stehman, S.: Evaluating Landsat and RapidEye
580 data for winter wheat mapping and area estimation in Punjab, Pakistan, *Remote Sensing*, 10, 489,
581 <https://doi.org/10.3390/rs10040489>, 2018.

582 Khan, A., Hansen, M. C., Potapov, P., Adusei, B., Stehman, S. V., and Steining, M. K.: An operational automated mapping
583 algorithm for in-season estimation of wheat area for Punjab, Pakistan, *International Journal of Remote Sensing*, 42, 3833–
584 3849, <https://doi.org/10.1080/01431161.2021.1883200>, 2021.

585 King, L., Adusei, B., Stehman, S. V., Potapov, P. V., Song, X.-P., Krylov, A., Di Bella, C., Loveland, T. R., Johnson, D. M.,
586 and Hansen, M. C.: A multi-resolution approach to national-scale cultivated area estimation of soybean, *Remote Sensing of
587 Environment*, 195, 13–29, <https://doi.org/10.1016/j.rse.2017.03.047>, 2017.

588 Konduri, V. S., Kumar, J., Hargrove, W. W., Hoffman, F. M., and Ganguly, A. R.: Mapping crops within the growing season
589 across the United States, *Remote Sensing of Environment*, 251, <https://doi.org/10.1016/j.rse.2020.112048>, 2020.

590 Lambert, M.-J., Traoré, P. C. S., Blaes, X., Baret, P., and Defourny, P.: Estimating smallholder crops production at village
591 level from Sentinel-2 time series in Mali's cotton belt, *Remote Sensing of Environment*, 216, 647–657,
592 <https://doi.org/10.1016/j.rse.2018.06.036>, 2018.

- 593 Lark, T. J., Spawn, S. A., Bougie, M., Gibbs, H. K., Lark, T. J., Spawn, S. A., Bougie, M., and Gibbs, H. K.: Cropland
594 expansion in the United States produces marginal yields at high costs to wildlife, *Nature Communications*, 11,
595 <https://doi.org/10.1038/s41467-020-18045-z>, 2020.
- 596 Larsen, A. E., Hendrickson, B. T., Dedeic, N., and MacDonald, A. J.: Taken as a given: Evaluating the accuracy of remotely
597 sensed crop data in the USA, *Agricultural Systems*, 141, 121–125, <https://doi.org/10.1016/j.agsy.2015.10.008>, 2015.
- 598 Li, H., Song, X.-P., Hansen, M. C., Becker-Reshef, I., Adusei, B., Pickering, J., Wang, L., Wang, L., Lin, Z., Zalles, V.,
599 Potapov, P., Stehman, S. V., and Justice, C.: Development of a 10-m resolution maize and soybean map over China: Matching
600 satellite-based crop classification with sample-based area estimation, *Remote Sensing of Environment*, 294,
601 <https://doi.org/10.1016/j.rse.2023.113623>, 2023.
- 602 Li, H., Song, X.-P., Adusei, B., Pickering, J., Lima, A., Poulson, A., Baggett, A., Potapov, P., Khan, A., Zalles, V., Hernandez-
603 Serna, A., Jantz, S. M., Pickens, A. H., Ortiz-Dominguez, C., Li, X., Kerr, T., Song, Z., Turubanova, S., Bongwele, E., Koy
604 Kondjo, H., Komarova, A., Stehman, S. V., and Hansen, M. C.: 2019-2022 10-m maize and soybean maps over the United
605 States, <https://doi.org/10.6084/m9.figshare.28934993.v1>, 2025.
- 606 Li, X.-Y., Li, X., Fan, Z., Mi, L., Kandakji, T., Song, Z., Li, D., and Song, X.-P.: Civil war hinders crop production and
607 threatens food security in Syria, *Nature Food*, 3, 38–46, <https://doi.org/10.1038/s43016-021-00432-4>, 2022.
- 608 Lin, C., Zhong, L., Song, X.-P., Dong, J., Lobell, D. B., and Jin, Z.: Early- and in-season crop type mapping without current-
609 year ground truth: Generating labels from historical information via a topology-based approach, *Remote Sensing of
610 Environment*, 274, <https://doi.org/10.1016/j.rse.2022.112994>, 2022.
- 611 Lin, F., Li, X., Jia, N., Feng, F., Huang, H., Huang, J., Fan, S., Ciaï, P., and Song, X.-P.: The impact of Russia-Ukraine
612 conflict on global food security, *Global Food Security*, 36, 100661, <https://doi.org/10.1016/j.gfs.2022.100661>, 2023.
- 613 Lobell, D. B., Deines, J. M., and Tommaso, S. D.: Changes in the drought sensitivity of US maize yields, *Nature Food*, 1, 729–
614 735, <https://doi.org/10.1038/s43016-020-00165-w>, 2020.
- 615 Lowder, S. K., Skoet, J., and Raney, T.: The number, size, and distribution of farms, smallholder farms, and family farms
616 worldwide, *World Development*, 87, 16–29, <https://doi.org/10.1016/j.worlddev.2015.10.041>, 2016.
- 617 Luo, Y., Zhang, Z., Zhang, L., Han, J., Cao, J., and Zhang, J.: Developing high-resolution crop maps for major crops in the
618 European Union based on transductive transfer learning and limited ground data, *Remote Sensing*, 14, 1809,
619 <https://doi.org/10.3390/rs14081809>, 2022.
- 620 Malingreau, J.-P.: Global vegetation dynamics: Satellite observations over Asia, *International Journal of Remote Sensing*, 7,
621 1121–1146, <https://doi.org/10.1080/01431168608948914>, 1986.
- 622 Manoochehr, S., Khoshmanesh, M., Ojha, C., Werth, S., Kerner, H., Grace Carlson, Sonam Futi Sherpa, Guang Zhai, and Jui-
623 Chi Lee: Persistent impact of spring floods on crop loss in U.S. Midwest, *Weather and Climate Extremes*, 34,
624 <https://doi.org/10.1016/j.wace.2021.100392>, 2021.
- 625 Marin, F. R., Zanon, A. J., Monzon, J. P., Andrade, J. F., Silva, E. H. F. M., Richter, G. L., Antolin, L. A. S., Ribeiro, B. S.
626 M. R., Ribas, G. G., Battisti, R., Heinemann, A. B., and Grassini, P.: Protecting the Amazon forest and reducing global
627 warming via agricultural intensification, *Nature Sustainability*, 1–9, <https://doi.org/10.1038/s41893-022-00968-8>, 2022.

628 Massey, R., Sankey, T. T., Congalton, R. G., Yadav, K., Thenkabail, P. S., Ozdogan, M., and Sánchez Meador, A. J.: MODIS
629 phenology-derived, multi-year distribution of conterminous U.S. crop types, *Remote Sensing of Environment*, 198, 490–503,
630 <https://doi.org/10.1016/j.rse.2017.06.033>, 2017.

631 Mei, Q., Zhang, Z., Han, J., Song, J., Dong, J., Wu, H., Xu, J., and Tao, F.: ChinaSoyArea10m: A dataset of soybean-planting
632 areas with a spatial resolution of 10 m across China from 2017 to 2021, *Earth System Science Data*, 16, 3213–3231,
633 <https://doi.org/10.5194/essd-16-3213-2024>, 2024.

634 Nafziger, E., Early-season soybean management for 2019: [https://farmdoc.illinois.edu/field-crop-](https://farmdoc.illinois.edu/field-crop-production/crop_production/early-season-soybean-management-for-2019.html)
635 [production/crop_production/early-season-soybean-management-for-2019.html](https://farmdoc.illinois.edu/field-crop-production/crop_production/early-season-soybean-management-for-2019.html), last access: 20 June 2024.

636 NASS CPR, Crop Progress Report: https://www.nass.usda.gov/Publications/National_Crop_Progress/, last access: 20 June
637 2024.

638 Olofsson, P., Foody, G. M., Stehman, S. V., and Woodcock, C. E.: Making better use of accuracy data in land change studies:
639 Estimating accuracy and area and quantifying uncertainty using stratified estimation, *Remote Sensing of Environment*, 129,
640 122–131, <https://doi.org/10.1016/j.rse.2012.10.031>, 2013.

641 Ouyang, Z., Jackson, R. B., McNicol, G., Fluet-Chouinard, E., Runkle, B. R. K., Papale, D., Knox, S. H., Cooley, S., Delwiche,
642 K. B., Feron, S., Irvin, J. A., Malhotra, A., Muddasir, M., Sabbatini, S., Alberto, M. C. R., Cescatti, A., Chen, C.-L., Dong, J.,
643 Fong, B. N., Guo, H., Hao, L., Iwata, H., Jia, Q., Ju, W., Kang, M., Li, H., Kim, J., Reba, M. L., Nayak, A. K., Roberti, D. R.,
644 Ryu, Y., Swain, C. K., Tsuang, B., Xiao, X., Yuan, W., Zhang, G., and Zhang, Y.: Paddy rice methane emissions across
645 Monsoon Asia, *Remote Sensing of Environment*, 284, 113335, <https://doi.org/10.1016/j.rse.2022.113335>, 2023.

646 Ozdogan, M. and Woodcock, C. E.: Resolution dependent errors in remote sensing of cultivated areas, *Remote Sensing of*
647 *Environment*, 103, 203–217, <https://doi.org/10.1016/j.rse.2006.04.004>, 2006.

648 Potapov, P., Hansen, M. C., Kommareddy, I., Kommareddy, A., Turubanova, S., Pickens, A., Adusei, B., Tyukavina, A., and
649 Ying, Q.: Landsat analysis ready data for global land cover and land cover change mapping, *Remote Sensing*, 12, 426,
650 <https://doi.org/10.3390/rs12030426>, 2020.

651 Potapov, P., Turubanova, S., Hansen, M. C., Tyukavina, A., Zalles, V., Khan, A., Song, X.-P., Pickens, A., Shen, Q., and
652 Cortez, J.: Global maps of cropland extent and change show accelerated cropland expansion in the twenty-first century, *Nature*
653 *Food*, 3, 19–28, <https://doi.org/10.1038/s43016-021-00429-z>, 2021a.

654 Potapov, P., Li, X., Hernandez-Serna, A., Tyukavina, A., Hansen, M. C., Kommareddy, A., Pickens, A., Turubanova, S., Tang,
655 H., Silva, C. E., Armston, J., Dubayah, R., Blair, J. B., and Hofton, M.: Mapping global forest canopy height through
656 integration of GEDI and Landsat data, *Remote Sensing of Environment*, 253, <https://doi.org/10.1016/j.rse.2020.112165>,
657 2021b.

658 Probst, P., Wright, M. N., and Boulesteix, A.-L.: Hyperparameters and tuning strategies for random forest, *Wiley*
659 *Interdisciplinary Reviews: Data Mining and Knowledge Discovery*, 9, e1301, <https://doi.org/10.1002/widm.1301>, 2019.

660 Remelgado, R., Zaitov, S., Kenjabayev, S., Stulina, G., Sultanov, M., Ibrakhimov, M., Akhmedov, M., Dukhovny, V., and
661 Conrad, C.: A crop type dataset for consistent land cover classification in Central Asia, *Scientific Data*, 7, 250,
662 <https://doi.org/10.1038/s41597-020-00591-2>, 2020.

663 Roy, D. P., Li, Z., and K. Zhang, H.: Adjustment of Sentinel-2 Multi-Spectral Instrument (MSI) red-edge band reflectance to
664 nadir BRDF adjusted reflectance (NBAR) and quantification of red-edge band BRDF Effects, *Remote Sensing*, 9,
665 <https://doi.org/10.3390/rs9121325>, 2017a.

- 666 Roy, D. P., Li, J., Zhang, H. K., Yan, L., Huang, H., and Li, Z.: Examination of Sentinel-2A multi-spectral instrument (MSI)
667 reflectance anisotropy and the suitability of a general method to normalize MSI reflectance to nadir BRDF adjusted reflectance,
668 *Remote Sensing of Environment*, 199, 25–38, <https://doi.org/10.1016/j.rse.2017.06.019>, 2017b.
- 669 Som-ard, J., Immitzer, M., Vuolo, F., Ninsawat, S., and Atzberger, C.: Mapping of crop types in 1989, 1999, 2009 and 2019
670 to assess major land cover trends of the Udon Thani Province, Thailand, *Computers and Electronics in Agriculture*, 198,
671 107083, <https://doi.org/10.1016/j.compag.2022.107083>, 2022.
- 672 Song, X. P., Hansen, M. C., Stehman, S. V., Potapov, P. V., Tyukavina, A., Vermote, E. F., and Townshend, J. R.: Global land
673 change from 1982 to 2016, *Nature*, 560, 639–643, <https://doi.org/10.1038/s41586-018-0411-9>, 2018.
- 674 Song, X.-P., Potapov, P. V., Krylov, A., King, L., Di Bella, C. M., Hudson, A., Khan, A., Adusei, B., Stehman, S. V., and
675 Hansen, M. C.: National-scale soybean mapping and area estimation in the United States using medium resolution satellite
676 imagery and field survey, *Remote Sensing of Environment*, 190, 383–395, <https://doi.org/10.1016/j.rse.2017.01.008>, 2017.
- 677 Song, X.-P., Huang, W., Hansen, M. C., and Potapov, P.: An evaluation of Landsat, Sentinel-2, Sentinel-1 and MODIS data
678 for crop type mapping, *Science of Remote Sensing*, 3, 100018, <https://doi.org/10.1016/j.srs.2021.100018>, 2021a.
- 679 Song, X.-P., Hansen, M. C., Potapov, P., Adusei, B., Pickering, J., Adami, M., Lima, A., Zalles, V., Stehman, S. V., Di Bella,
680 C. M., Conde, M. C., Copati, E. J., Fernandes, L. B., Hernandez-Serna, A., Jantz, S. M., Pickens, A. H., Turubanova, S., and
681 Tyukavina, A.: Massive soybean expansion in South America since 2000 and implications for conservation, *Nature*
682 *Sustainability*, 4, 784–792, <https://doi.org/10.1038/s41893-021-00729-z>, 2021b.
- 683 Song, X.-P., Li, H., Potapov, P., and Hansen, M. C.: Annual 30 m soybean yield mapping in Brazil using long-term satellite
684 observations, climate data and machine learning, *Agricultural and Forest Meteorology*, 326,
685 <https://doi.org/10.1016/j.agrformet.2022.109186>, 2022.
- 686 Stehman, S. V.: Estimating area and map accuracy for stratified random sampling when the strata are different from the map
687 classes, *International Journal of Remote Sensing*, 35, 4923–4939, <https://doi.org/10.1080/01431161.2014.930207>, 2014.
- 688 Tanaka, T., Sun, L., Becker-Reshef, I., Song, X.-P., and Puricelli, E.: Satellite forecasting of crop harvest can trigger a cross-
689 hemispheric production response and improve global food security, *Communications Earth & Environment*, 4, 334,
690 <https://doi.org/10.1038/s43247-023-00992-2>, 2023.
- 691 Van Tricht, K., Degerickx, J., Gilliams, S., Zanaga, D., Battude, M., Grosu, A., Brombacher, J., Lesiv, M., Bayas, J. C. L.,
692 Karanam, S., Fritz, S., Becker-Reshef, I., Franch, B., Mollà-Bononad, B., Boogaard, H., Pratihast, A. K., Koetz, B., and
693 Szantoi, Z.: WorldCereal: A dynamic open-source system for global-scale, seasonal, and reproducible crop and irrigation
694 mapping, *Earth System Science Data*, 15, 5491–5515, <https://doi.org/10.5194/essd-15-5491-2023>, 2023.
- 695 Wang, S., Azzari, G., and Lobell, D. B.: Crop type mapping without field-level labels: Random forest transfer and unsupervised
696 clustering techniques, *Remote Sensing of Environment*, 222, 303–317, <https://doi.org/10.1016/j.rse.2018.12.026>, 2019.
- 697 Wang, S., Di Tommaso, S., Deines, J. M., and Lobell, D. B.: Mapping twenty years of corn and soybean across the US Midwest
698 using the Landsat archive, *Scientific Data*, 7, 307, <https://doi.org/10.1038/s41597-020-00646-4>, 2020.
- 699 Wang, Y., Feng, K., Sun, L., Xie, Y., and Song, X.-P.: Satellite-based soybean yield prediction in Argentina: A comparison
700 between panel regression and deep learning methods, *Computers and Electronics in Agriculture*, 221, 108978,
701 <https://doi.org/10.1016/j.compag.2024.108978>, 2024.

702 Wardlow, B. D. and Egbert, S. L.: Large-area crop mapping using time-series MODIS 250 m NDVI data: An assessment for
703 the U.S. Central Great Plains, *Remote Sensing of Environment*, 112, 1096–1116, <https://doi.org/10.1016/j.rse.2007.07.019>,
704 2008.

705 Wardlow, B. D., Egbert, S. L., and Kastens, J. H.: Analysis of time-series MODIS 250 m vegetation index data for crop
706 classification in the U.S. Central Great Plains, *Remote Sensing of Environment*, 108, 290–310,
707 <https://doi.org/10.1016/j.rse.2006.11.021>, 2007.

708 Woodcock, C. E., Allen, R., Anderson, M., Belward, A., Bindschadler, R., Cohen, W., Gao, F., Goward, S. N., Helder, D.,
709 Helmer, E., Nemani, R., Oreopoulos, L., Schott, J., Thenkabail, P. S., Vermote, E. F., Vogelmann, J., Wulder, M. A., and
710 Wynne, R.: Free access to Landsat imagery, *Science*, 320, 1011, <https://doi.org/10.1126/science.320.5879.1011a>, 2008.

711 Wright, C. K. and Wimberly, M. C.: Recent land use change in the Western Corn Belt threatens grasslands and wetlands,
712 *Proceedings of the National Academy of Sciences*, 110, 4134–4139, <https://doi.org/10.1073/pnas.1215404110>, 2013.

713 Xiong, J., Thenkabail, P. S., Gumma, M. K., Teluguntla, P., Poehnelt, J., Congalton, R. G., Yadav, K., and Thau, D.:
714 Automated cropland mapping of continental Africa using Google Earth Engine cloud computing, *ISPRS Journal of*
715 *Photogrammetry and Remote Sensing*, 126, 225–244, <https://doi.org/10.1016/j.isprsjprs.2017.01.019>, 2017.

716 Yan, L. and Roy, D. P.: Automated crop field extraction from multi-temporal Web Enabled Landsat Data, *Remote Sensing of*
717 *Environment*, 144, 42–64, <https://doi.org/10.1016/j.rse.2014.01.006>, 2014.

718 Yan, L. and Roy, D. P.: Conterminous United States crop field size quantification from multi-temporal Landsat data, *Remote*
719 *Sensing of Environment*, 172, 67–86, <https://doi.org/10.1016/j.rse.2015.10.034>, 2016.

720 Yang, Y., Wilson, L. T., and Wang, J.: A spatially explicit crop planting initiation and progression model for the conterminous
721 United States, *European Journal of Agronomy*, 90, 184–197, <https://doi.org/10.1016/j.eja.2017.08.004>, 2017.

722 Yang, Z., Diao, C., and Gao, F.: Towards scalable within-season crop mapping with phenology normalization and deep
723 learning, *IEEE Journal of Selected Topics in Applied Earth Observations and Remote Sensing*, 16, 1390–1402,
724 <https://doi.org/10.1109/JSTARS.2023.3237500>, 2023.

725 You, N., Dong, J., Huang, J., Du, G., Zhang, G., He, Y., Yang, T., Di, Y., and Xiao, X.: The 10-m crop type maps in Northeast
726 China during 2017–2019, *Scientific Data*, 8, 41, <https://doi.org/10.1038/s41597-021-00827-9>, 2021.

727 You, N., Dong, J., Li, J., Huang, J., and Jin, Z.: Rapid early-season maize mapping without crop labels, *Remote Sensing of*
728 *Environment*, 290, <https://doi.org/10.1016/j.rse.2023.113496>, 2023.

729 Zalles, V., Hansen, M. C., Potapov, P. V., Stehman, S. V., Tyukavina, A., Pickens, A., Song, X. P., Adusei, B., Okpa, C.,
730 Aguilar, R., John, N., and Chavez, S.: Near doubling of Brazil’s intensive row crop area since 2000, *Proceedings of the National*
731 *Academy of Sciences*, 116, 428–435, <https://doi.org/10.1073/pnas.1810301115>, 2019.

732 Zalles, V., Hansen, M. C., Potapov, P. V., Parker, D., Stehman, S. V., Pickens, A. H., Parente, L. L., Ferreira, L. G., Song, X.-
733 P., Hernandez-Serna, A., and Kommareddy, I.: Rapid expansion of human impact on natural land in South America since
734 1985, *Science Advances*, 7, eabg1620, <https://doi.org/10.1126/sciadv.abg1620>, 2021.

735 Zhong, L., Gong, P., and Biging, G. S.: Efficient corn and soybean mapping with temporal extendability: A multi-year
736 experiment using Landsat imagery, *Remote Sensing of Environment*, 140, 1–13, <https://doi.org/10.1016/j.rse.2013.08.023>,
737 2014.

738 Zhu, Z., Wang, S., and Woodcock, C. E.: Improvement and expansion of the Fmask algorithm: Cloud, cloud shadow, and
739 snow detection for Landsats 4-7, 8, and Sentinel 2 images, *Remote Sensing of Environment*, 159, 269-277,
740 <https://doi.org/10.1016/j.rse.2014.12.014>, 2015.